https://doi.org/10.1016/j.jcsr.2022.107343

Experimental investigations on material properties and stub column behaviour of high strength steel irregular hexagonal hollow sections

Jun-zhi Liu[1]; Han Fang[2]; Tak-Ming Chan[1,3] *

[1] Department of Civil and Environmental Engineering, The Hong Kong Polytechnic University, Hong Kong, China

[2] School of Civil Engineering, University of Leeds, United Kingdom (formerly, School of Civil, Environmental and Mining Engineering, The University of Adelaide, South Australia 5005, Australia)

[3] Chinese National Engineering Research Centre for Steel Construction (Hong Kong Branch), The Hong Kong Polytechnic University, Hong Kong, China

* Corresponding author: tak-ming.chan@polyu.edu.hk

Abstract

Comprehensive experimental investigations into the material properties and stub column behaviour of cold-formed high strength steel (HSS) irregular hexagonal hollow sections (IHexHS) are presented in this paper. Apart from the tensile coupons taken from the parent plates, tensile coupons extracted from the flat and corner portions from the cross-sections were also tested in order to measure the effect of the fabrication process on material properties. The strength enhancement predictive models proposed by previous studies were compared with the obtained test results from corner coupons with increased strength due to the cold-forming effect. A total of 20 HSS IHexHS stub column specimens were tested under axial compression and the cross-section classification from the existing structural steel design codes of EN 1993-1-12, ANSI/AISC 360-16, AS 4100, AISI S100-16 and design approaches of DSM and CSM were compared and assessed against the obtained results. It was found that the design provisions of cross-section classification in current design codes cannot be extended to the HSS IHexHS stub columns. Based on current codified yield slenderness limits, the strength predictions from design codes exhibit conservatism without the consideration of strain hardening and beneficial effect of element interaction whereas cross-sections with intermediate slenderness values were over-predicted.

Keywords: Irregular hexagonal sections; Local buckling behaviour; Cold-forming effect; High strength steel; Design methods.

1. Introduction

With the advancement in production technology and welding techniques, high strength steel (HSS), generally defined by the nominal yield strength equal or greater than 460 MPa, have been produced with acceptable ductility and weldability [1–2]. In comparison with the normal strength steel (NSS), HSS offers numerous benefits including higher yield strength and higher strength-to-weight ratio, which enable realization of lighter structural components with reduced member sizes. The application of HSS also facilitates the scheme of environmental and ecological sustainable development due to the reduced transportation cost and less welding work resulting in decreased carbon dioxide emissions. These advantages make HSS popular in the construction of high-rise buildings and long-span structures. In China, several large-span structures have been constructed with HSS, such as the public buildings of National stadium (Bird's nest), CCTV

headquarters and Phoenix international media center where HSS with nominal yield strength of 460 MPa are used, as shown in Fig. 1(a). HSS have also been widely applied in bridges, such as the Tseung Kwan O bridge in Hong Kong in which HSS with steel grade of Q690 is used, as shown in Fig. 1(b).

In terms of the material properties, those for HSS are primarily affected by the chemical compositions, heat treatment and manufacturing processes [5]. Two types of heat treatment are commonly used to produce HSS plates, namely thermomechanical rolling and quench and tempering, which lead to increment in material strength without overly compromising the ductility, weldability and toughness [6]. With the development of the welding technologies, HSS plates can be welded into different shapes. Sections comprising the individual HSS plates which were welded separately are called built-up sections (or welded sections). In the past years, research efforts have been made focusing on conventional tubular profile such as HSS built-up box sections [7–14]. Local buckling behaviour of the welded box sections made up from HT80 with nominal yield strength of 690 MPa were studied by Usami and Fukumoto [7]. The welded box-sections fabricated by HSS plate of BISALLOY80 with nominal yield strength of 690 MPa were tested under axial compression, by which the local and overall buckling behaviours have been investigated [8]. Clarin [9] conducted stub column tests to study the local buckling behaviour of the welded box sections comprising three different strength grades of DOMEX 420 (nominal yield strength f_y = 420 MPa), WELDOX 700 (nominal yield strength f_y = 700 MPa) and WELDOX 1100 (nominal yield strength f_y = 1100 MPa). Local buckling behaviour of the welded box sections made up from the high strength low alloy steel of 18Mn2CrMoBA have also been studied by Gao et al. [10] with nominal yield strength varying between 745 MPa and 800 MPa. Design provisions from AISC 360 have been compared and assessed on the HSS welded box sections stub column with nominal yield strength of 800MPa by Kim et al. [11]. Shi et al. [12] carried out experimental investigations on welded box and I-sections made up from Q460 steel with nominal yield strength of 460 MPa, demonstrating the deficiencies of the current design provisions to HSS sections. Local buckling and interaction of the local buckling and overall buckling of the welded box sections made of HSS were also examined by Schillo and Feldmann [13-14], with S500 and S960 steel with nominal yield strength of 500 MPa and 960 MPa respectively. In addition to the built-up sections, hot-finished sections of square hollow sections (SHS) and rectangular hollow sections (RHS) have also been studied focusing on the local buckling behaviour [15–16].

Compared with built-up or hot-finished sections, cold-formed HSS hollow sections have great potential in structural engineering due to their ease of fabrication, less energy consumption, lightweight members with higher strength due to the cold-forming processes. Investigations have been conducted on cold-formed HSS tubular sections including square hollow sections (SHS), rectangular hollow sections (RHS) and circular sections (CHS) [17–20]. Apart from these conventional cross-section profile, increasing interests have been made focusing on the applications of polygonal sections such as HSS hexagonal hollow sections (HexHS) and octagonal hollow sections (OctHS). Compared with the conventional layout of CHS, polygonal hollow sections, such as HexHS and OctHS, provide the flat surface which can allow for easier connection construction with incoming members, particular in the application of the modular integrated construction, which propose higher requirement on the connection possibility. Meanwhile, HexHS and OctHS resemble their CHS counterpart more rather than SHS, which indicate that better local buckling resistance and enhanced confinement can be provided [21–26]. In particular, the application of irregular hexagonal sections (IHexHS) as part of the polygonal section family was successfully applied in the high-rise buildings of CITIC tower in Beijing with total height of 528 meters and Gaoyin Finance Building in Tianjin with total

height of 597 meters as the mega columns connecting the trusses and braces [27]. The material properties variation and residual stresses distribution have been investigated for HSS cold-formed IHexHS [28]. However, there is no experimental data available for stub column behaviour of HSS cold-formed IHexHS. It is thereby of vital importance to conduct the investigation for better understanding the structural behavior of HSS cold-formed IHexHS, by which the safe and efficient design provisions can be determined.

It is known that HSS conventional cross-sections such as HSS RHS and CHS are covered by design codes of EN 1993-1-12 [29], AISI/AISC 360-16 [30] and AS 4100 [31]. The Eurocode of EN 1993-1-12 [29] is applicable to the HSS up to strength grade of S700 and the North American code of AISI/AISC 360-16 [30] encompasses the structural steel design with nominal yield strength up to 690 MPa. Note however that stringent requirements are specified for hollow sections that only sections with nominal yield strength less than 485 MPa are allowed to follow the design provisions in this code. AS 4100 [31] covers structural steel design with nominal yield strength up to 690 MPa except for hollow sections. The provisions stipulate that the hollow sections with nominal yield strength greater than 450 MPa are beyond the scope of the code, implying that these design provisions are only applicable to HSS tubular hollow sections with nominal yield strength not greater than 450 MPa. Furthermore, design specifications of HSS IHexHS are not provided in existing structural steel design codes. Whether the current structural steel design codes can be extended to cover the design of HSS IHexHS is unknown. Thus, there is a need to assess the applicability of the existing design codes for conventional profiled sections to the HSS HexHS in this study.

To address these research gaps, a comprehensive experimental programme was carried out by testing 20 HSS cold-formed IHexHS stub columns with a spectrum of cross-section dimensions (plate width to thickness ratio) varying from 3.8 to 34.5. The material properties for each specimen were measured through tensile coupon tests. The tensile coupons were taken from both the parent plates and the sections of HSS IHexHS. The measurements of the initial local geometric imperfections were also conducted. The local buckling behaviour and the cross-section resistance were investigated under axial concentric compression. The obtained experimental results were assessed against the cross-section classification in the existing codes of practice. The developed design approaches such as the direct strength method (DSM) [32] and continuous strength method (CSM) [33] were also discussed and assessed for HSS IHexHS.

2. Test specimens

A total of 20 HSS cold-formed IHexHS stub column specimens under axial compression were prepared. HSS plates of Q690 with two nominal thicknesses of 6 mm and 10 mm were used for preparing the HSS cold-formed IHexHS specimens. The cold-formed HSS IHexHS in this study were fabricated by welding two half-sections through Gas Metal Arc Welding (GMAW) in longitudinal direction with each half-section featuring one corner of 90 degrees and the other two corners of 135 degrees through press-braking, as shown in Fig. 2. To avoid the cracking along the bending area due to the highly concentrated stress during press-braking, the designed inner radius-to-thickness ratios were carefully designed to meet the requirements proposed in cold-formed steel specification in EN 10219-2 [34]. The inner corner radius to thickness ratio is three for all the investigated IHexHS and no cracks were observed at the surface of the specimen. The 1.2 mm electrode of ER110S-G category (f_y = 860 MPa, f_u = 920MPa) in accordance with the specification AWS A5.28/5.28 M [35] was used to achieve the overmatched condition.

The dimensions of the cross-section for HSS cold-formed IHexHS were measured using the symbols shown in Fig. 2. The detailed definition of the symbols of the cross section are illustrated in Fig. 3, where H is the height of the cross section, B is the outer width of the IHexHS, B_L is the longer edge length of the IHexHS, b_L is the clear width of the vertical flat portion with welding bead excluding the corner regions, B_s is the shorter edge length, b_s is the clear width of an inclined short flat side excluding the corner portions, t is the nominal thickness of the cross section, r_o and r_i are the outer and inner corner radius of the cross section respectively. The specimen label system including detailed information about the nominal cross section geometry is utilized throughout the paper. Following the cross-sectional shape of the specimen "IHex", the nominal dimensions (B_L × t) of the HSS IHexHS is denoted after the hyphen with nominal aspect ratio given after geometries, and the symbol of "#" is used to indicate the repeated tests. For example, the specimen of "IHex-125 × 6-1.80#" indicates a repeated specimen with nominal edge length B_L of 125 mm, nominal thickness of 6 mm and nominal aspect ratio of 1.80. The measured dimensions of the specimens are presented in Table 1. The thickness t of the HSS cold-formed IHexHS was conventionally measured at the end sections using the digital Vernier caliper and the thickness along the specimen length was measured using an ultrasonic measurement gauge with measured locations shown in Fig. 4. The measured data were averaged and presented in Table 1.

3. Material properties

3.1. Tensile coupon tests

To acquire the material properties of the HSS cold-formed IHexHS, tensile coupon tests were conducted on tensile coupons extracted from both the parent plates and the cross-sections of IHexHS from three critical locations, namely the flat portion and the corner portions (one with 90 degree and the other is 135 degree). Twelve tensile coupons were machined longitudinally and transversely from the parent plates with six for each thickness plate respectively. Fifteen flat- and twenty corner tensile coupons were taken from the flat portion and corner portions of HSS cold-formed IHexHS as shown in Fig. 2. To limit the cold-forming effect, the flat coupons were extracted from corner regions at a distance of at least 3t. Analogous to the specimen labeling system, the tensile coupons were labelled in a form of "IHex-nominal edge length B_L × nominal thickness t-nominal aspect ratio-corner angle" for corner coupons and "IHex-nominal edge length B_L × nominal thickness t-nominal aspect ratio" for flat coupons. For instance, IHex-160×6-1.90-90 indicates a corner coupon taken from the corner portion of HSS cold-formed IHexHS of "IHex-160×6-1.90".

The tensile coupon tests were conducted in accordance with EN 6892-1: 2019 [36] and an in-house electromechanical high force universal testing system of Instron 5982 testing machine with a capacity of 100 kN and an optical non-contact video extensometer was used to record the full engineering stress-strain relationship. Test arrangement for the tensile coupon tests for flat coupons and corner coupons are given in Fig. 5 and the detailed testing procedure for tensile coupon tests are referred to [28]. The dimensions of the tensile coupons were carefully designed in accordance with the codified specifications in EN 6892-1: 2019 [36]. The parent coupons were featured with 13 mm and 8 mm width along a gauge length of 50 mm for 6 mm and 10 mm thick plates respectively. In addition, the flat- and corner tensile coupons were machined with 4 mm width along the gauge length of 25 mm from the sections with the plate thicknesses of 6 mm. With regards to the tensile coupons taken from sections with the plate thickness of 10 mm, the width of the specimen was 8 mm along the gauge length of 50 mm. Special attention was also paid to the corner coupons,

and a pair of specially developed grips with two pins was utilized to apply the tensile load through the holes drilled at the distance of 20 mm from the end of the coupon with diameter of 10 mm.

Some of the failed tensile coupons with fracture in the parallel gauge length are presented in Fig. 6. The measured material properties for parent plates are summarized in Table 2, where $E_{s,p}$ indicates the elastic modulus of the parent steel plate, $f_{y,p}$ is yield strength, $f_{u,p}$ is the ultimate strength, $\varepsilon_{sh,p}$ is strain-hardening strain, $\varepsilon_{u,p}$ is strain at ultimate strength, $\varepsilon_{f,p}$ is elongation at fracture and ν is Poisson's ratio. Test results of the material properties of the flat- and corner coupons taken from the sections are summarized in Table 3 and Table 4. Apart from the basic material properties, 0.05% proof strength for flat and corner coupons are also provided in Table 3 and Table 4. The letters "f" and "c" in the subscript indicate that the material properties are obtained from flat coupons and corner coupons respectively.

3.2. Assessment of the material properties and ductility requirements

The determined stress-strain curves from the parent plates are plotted in Figs. 7–8. The stress-strain curves of the flat coupons and corner coupons taken from the HSS cold-formed IHexHS of IHex-125×6-1.60 is presented in Fig. 9 to illustrate the effect of the press-braking process on the material strength. It can be observed that both yield strength and ultimate strength from the corner coupons are improved significantly compared with the flat coupon due to the excessive strain hardening. The ductility is decreased with lower elongation at fracture and ultimate strain. Moreover, ultimate strength is slightly higher for the corner coupon with an angle of 90 degrees, which may attribute to the more severer plastic deformation subject to press-braking compared with the counterpart with 135 degrees.

Ductility requirements for structural steel design are set out in Eurocode EN 1993-1-1 [37] for the steel with nominal yield strength not greater than 460 MPa, the ductility requirements are specified as follows,

i) $f_u/f_y \geq 1.10$
ii) $\varepsilon_f \geq 15\%$
iii) $\varepsilon_u/\varepsilon_y \geq 15$

In addition to the EN 1993-1-1 [37], ductility requirements are also specified in UK National Annex to EN 1993-1-1 [38]. The requirements are more stringent in the UK National Annex for plastic design which requires the ratio of ultimate strength to yield strength no less than 1.15, and the fracture strain should be no less than 20 times the yield strain. For higher strength steel up to S700, relaxed requirements are stipulated in EN 1993-1-12 [29]. These requirements are provided as follows,

i) $f_u/f_y \geq 1.05$
ii) $\varepsilon_f \geq 10\%$
iii) $\varepsilon_u/\varepsilon_y \geq 15$

Likewise, the UK National Annex to the EN 1993-1-12 [39] specifies more stringent requirements than the EN 1993-1-12 [29], the requirement on the ratio of ultimate strength to yield strength is same as the one set out in EN 1993-1-1 [38], the requirement on the ratio of the ultimate strain to yield strain is differentiated in elastic design and plastic design, given as follows,

i) $f_u/f_y \geq 1.10$
ii) $\varepsilon_f \geq 10\%$
iii) $\varepsilon_u/\varepsilon_y \geq 20$ (plastic), $\varepsilon_u/\varepsilon_y \geq 15$ (elastic)

In Fig. 10, the material properties obtained from the tests are compared with the requirements set out in the design codes. It is observed that both flat coupons and corner coupons meet the requirements of the strength ratio specified in EN 1993-1-12 [39], except for two coupons which featured with f_u/f_y lower than 1.05. Comparison of the elongation at fracture against the limit values set out in design codes are plotted in Fig. 11. Most of the coupons meet the requirement except for two coupons exhibiting elongation of fracture lower than 10%. The elongation of fracture from corner coupons are significantly lower than flat coupons due to the cold-forming effect as discussed in previous sub-section of 3.1. Concerning the strain at failure, corner coupons cannot meet the requirements either from Eurocode or its UK National Annex due to the reduced ductility caused by press-braking, as shown in Fig. 12. The variations of f_u/f_y with the yield strength f_y for both flat coupons and corner coupons along with the empirical equation relating the ratio of f_u/f_y to f_y are plotted in Fig. 13. The empirical relationships were proposed by Fukumoto [40], Langenberg [41] and Garnder and Yun [42], as given by Eqs. (1) – (3) respectively.

$$\frac{f_u}{f_y} = 0.83 + \frac{203.8}{f_y} \quad (1)$$

$$\frac{f_u}{f_y} = [1 - 0.72e^{(0.0027 f_y)}]^{-1} \quad (2)$$

$$\frac{f_u}{f_y} = (1 + \frac{130}{f_y})^{1.4} \quad (3)$$

The empirical equation provided by Gardner and Yun [42] generate reasonable predictions for flat coupons whereas the expression provided by Fukumoto [40] and Langenberg [41] over-predicts the ratio of ultimate strength to yield strength. It is observed that all these three expressions yield non-conservative predictions for corner coupons which display lower ratio of f_u/f_y. Ultimate strain is another important material parameter to represent the ductility, and the ultimate strain is also necessary in design methods such as CSM. Hence, the ultimate strain obtained from the experimental tests were also compared with the predictive equations proposed by Gardner and Yun [42] and Liu et al. [2]. It is seen that the proposed model by Liu et al. [2] accurately predicts the ultimate strain of flat coupons and the empirical model from Gardner and Yun [42] provides underestimated results for flat coupons, as shown in Fig. 14. Both predictive equations generate over-conservative results for corner coupons, implying that suitable equation to represent the ultimate strain of the corner coupons which underwent excessive plastic deformation and strain hardening needs to be developed.

3.3. Strength enhancement due to press-braking

Upon the tensile coupon test results, it is noticed that manufacturing process of press-braking significantly

improve the yield strength and ultimate strength of the corner coupons. To have efficient and accurate design, explicitly accounting the enhanced material properties is necessary. The applicability of the current design methods for predicting the improved strength due to press-braking was assessed and compared against the test results. Predictive equations for the enhanced yield strength were provided by Karren [43] and later adopted in the AISI S100-16 [44], as follows,

$$f_{y,c} = \frac{B_c}{(r_i / t)^{\alpha}} f_y \quad (4)$$

$$B_c = 3.69\left(\frac{f_u}{f_y}\right) - 0.819\left(\frac{f_u}{f_y}\right)^2 - 1.79 \quad (5)$$

$$\alpha = 0.192\left(\frac{f_u}{f_y}\right) - 0.068 \quad (6)$$

Pham et al. [45] modified the coefficients of the predictive equations which were applicable to HSS cold-formed steel with nominal yield strength of 450 MPa. The modified coefficients are given by Eqs. (7) – (8)

$$B_c = 1.588\left(\frac{f_u}{f_y}\right) - 0.218\left(\frac{f_u}{f_y}\right)^2 - 0.038 \quad (7)$$

$$\alpha = 0.228\left(\frac{f_u}{f_y}\right) - 0.068 \quad (8)$$

The modified predictions taking the extended corner regions proposed by Gardner et al. [46] were also compared and assessed. Predictive equations with modified coefficients are given by Eqs. (9) – (10)

$$B_c = 2.9\left(\frac{f_u}{f_y}\right) - 0.752\left(\frac{f_u}{f_y}\right)^2 - 1.09 \quad (9)$$

$$\alpha = 0.23\left(\frac{f_u}{f_y}\right) - 0.011 \quad (10)$$

The measured yield strength for corner coupons were compared with the predicted enhanced yield strength due to press-braking. Statistical analysis and the comparison values using these design methods are tabulated in Table 5. The predicted yield strength was normalised to the yield strength of the parent plates. The normalised predicted values were compared with the normalised test results and plot in Fig. 15 along with two trendlines of 10%. Compared with the methods proposed by Pham et al. [45] and Gardner et al. [46], AISI S00-16 [44] provides the most accurate predictions with mean value of $f_{y,pred}/f_y$ equals to 0.98 and the corresponding CoV of 0.019. The mean values of $f_{y,pred}/f_y$ provides by the method of Pham et al. [45] and Gardner et al. [46] are 1.05 and 0.87 with CoV of 0.015 and 0.016 respectively. It is of worthy noted that over-conservative predictions are obtained based on the method from Gardner et al. [46] and over-predicted strength are generated from Pham et al. [45] method. To accurately predict the enhanced strength for the corner region of HSS cold-formed IHexHS subject to press-braking, a predictive model is proposed with modified coefficients as follows in Eqs. (11) – (12). The predicted results with improved accuracy can be observed in Fig. 15.

$$B_c = 3.65\left(\frac{f_u}{f_y}\right) - 0.81\left(\frac{f_u}{f_y}\right)^2 - 1.75 \quad (11)$$

$$\alpha = 0.18\left(\frac{f_u}{f_y}\right) - 0.082 \quad (12)$$

4. Geometric imperfection

4.1 Initial local geometric imperfection measurement

The initial geometric imperfections are known to be caused by manufacturing, transportation and installation. Measurements of initial local geometric imperfections were carried out for all the investigated HSS cold-formed IHexHS prior to testing. The experimental set-up used in this study was similar to that used by Schafer and Pekoz [47]. Each specimen was mounted to the bed of a milling machine as a measuring platform and its location was fixed to avoid any movement. Three Linear Variable Displacement Transducers (LVDTs) with an accuracy of 0.001 mm were affixed to the milling machine head with a clamper and two were positioned near the corners and one at the centerline of each surface, resulting in a total of eighteen runs per section, as shown in Fig. 16. To limit the effect of the end flaring and release of the residual stress effect, the LVDTs moving along the specimen the length started and finished at 50 mm away from the specimen ends, which was successfully applied in Chen et al. [48] and Liu et al. [49, 50].

4.2. Discussions on measurement results

The recorded data from the mid-portion of the flat surface was used to deduct the average data from the corners. The maximum value among all six surfaces were taken as the initial local geometric imperfection amplitude (ω_0) and amplitudes for all the 20 specimens are given in Table 6. A typical distribution of the initial local geometric imperfection for HSS IHexHS stub column of IHex-160×6-1.90 is presented in Fig. 17. The obtained imperfection values are also plotted against the cross-section slenderness $\overline{\lambda_p}$, as shown in Fig. 18(a). The cross-section slenderness was determined in accordance with the EN 1993-1-5 [51], taken as that of the slenderest constituent plate element. It is of worthy noted that the initial geometric imperfection values exhibit a tendency to increase as the cross-section slenderness increasing. EN 10219-2 [34] specifies the maximum out of flatness tolerances 0.8%B for cold-formed tubular sections, where B is the outer width of the cross section. The limit value was thus derived for both shorter and longer edge lengths, denoted as $\omega_{EN\text{-}S}$ and $\omega_{EN\text{-}L}$ respectively. The variations of the $\omega_0/\omega_{EN\text{-}S}$ is plotted against the cross-section slenderness since the more stringent tolerance limits were derived based on shorter edge length. It is seen in Fig. 18(b) that except for one specimen fail to meet this fabrication requirement, all the remaining specimens satisfy the design provisions. Moreover, the measured initial imperfections are also compared with the recommended imperfection amplitude b/200 set out in EN 1993-1-5 [51], denoted as $\omega_{EC3\text{-}5}$. Based on the comparisons shown in Fig. 18(c), the specified imperfection value can generally be applied to represent the initial imperfection geometric imperfection amplitude for HSS cold-formed IHexHS stub columns. A predictive model for the initial local geometric imperfections is proposed based on the obtained test results using the form proposed by Dawson and Walker [51], as shown in Eq. (13), where f_{cr} is the elastic local buckling stress

for the plate with the largest slenderness in a cross section. The coefficient of β is a constant and estimated to be 0.09 for the HSS cold-formed IHexHS through regression analysis, as shown in Fig. 19.

$$\omega_{\mathrm{D\&W}} = \beta \left(\frac{f_{\mathrm{y}}}{f_{\mathrm{cr}}}\right)^{0.5} t \tag{13}$$

5. Stub column tests

5.1 Test setup and procedure

A total of 20 HSS cold-formed IHexHS stub columns were tested under axial compressive load in order to examine the local buckling behaviour and cross-sectional resistance. The test set-up and instrumentation for the compression tests are shown in Fig. 20. The axial compressive loading was applied using a universal servo-controlled testing machine from POPWIL with the capacity of 25000 kN. Four 50 mm range Linear Variable Displacement Transducers (LVDTs) were positioned vertically to measure the axial end shortening of the stub columns. Moreover, a total of 10 strain gauges were adhered to the mid-height of each specimen at both flat and corner portions to measure the average compressive strain in the longitudinal direction and to detect the initiation of local buckling, if any. The location of the strain gauges for each specimen was arranged to explicitly reflect the difference of flat portion and corner portion under compression due to the distinct material properties across the section due to the press-braking process, as shown in Fig. 20(a). Prior to the compressive testing, section ends of the stub column specimens were milled flat to ensure a uniformly distributed load by well contacted fix boundary condition between the specimen and the hardened end plates [19, 21]. To prevent the premature local buckling failure at the section ends due to the highly concentrated loads, a pair of end stiffeners with 30 mm thick and 25 mm in height were designed to accommodate the stub column specimens and clamp tightly the end of the specimen using several high strength bolts as shown in Fig. 20(a) in the axonometric view. All the stub column tests were performed under displacement controlled at a constant loading rate of 0.05%L mm/min, which is similar to the loading speed applying for the tensile coupon tests. Initial loading tests (pre-loading) were performed for each stub column specimen prior to the compression tests up to 10% of the anticipated yield load to ensure the loading system and instrumentations working well. To eliminate the possible gap between the specimen and the bearing plate, initial load with an approximate value of 20 kN was applied to the specimens. Any possible gaps between the specimen and the bearing plate can be eliminated through the rotation of the spherical bearing on the top of the testing machine as shown in Fig. 20. Note that the LVDTs readings necessarily contain both the end shortening of the stub column specimen and the elastic deformation of the end plates as well as the bearing plate of the testing machine. The true end shortening of the stub column specimen was thus obtained using the strain gauge readings as well as the LVDTs readings by which the effect from the involved elastic deformations from end plates can be removed. The basic theory of this method is that the deformation of the end plates is elastically proportional to the applied axial load, the elastic coefficient can be determined from the readings from the LVDTs and strain gauges.

5.2 Test results

The obtained axial load-end shortening curves for HSS cold-formed IHexHS are plotted in Fig. 21. Key

experimental test results of the IHexHS stub column tests including the ultimate axial load N_u, the end shortening at ultimate load δ_u, yield load N_y and the ultimate to yield load ratio N_u/N_y are reported in Table 7. The ratio of ultimate load to yield load N_u/N_y was used to characterize whether the specimens are failed by cross-section yielding or local buckling. If the ratio of N_u/N_y is greater than the unity, the specimen is considered to fail by cross-section yielding, otherwise, the specimen fails by local buckling prior to the attainment of the sectional yield load. For those sections failed by cross-section yielding such as the specimens of IHex-70×6-1.45, IHex-70×6-1.50, IHex-70×6-1.55, IHex-70×6-1.60, IHex-150×10-1.70 IHex-160×10-1.50 and IHex-170×10-2.00, the load-end shortening curves exhibit pronounced deformation capacity and ductility as shown in Fig. 21. For those sections failed by local buckling, including the stub column specimens of IHex-125×6-1.80, IHex-125×6-1.60, IHex-150×6-1.80, IHex-160×6-1.90, IHex-165×6-1.85, IHex-185×6-2.15 and IHex-225×6-2.15, the load-end shortening curves are accompanied with relative sharp drop after achieving the ultimate resistance with limited deformation capacity and less ductility. This observation primarily attributes to the local buckling of the slender plate members which triggers the premature failure of the sections leading to the early drop in load-end shortening curves. The relationship of the normalised load N_u/Af_y and normalised end shortening (δ_u/L) curves for all the investigated stub columns are plotted in Fig. 22, where N_u is the ultimate load from the test, A is the gross area of the cross-section, f_y is the measured yield strength from flat portion, δ_u is the measured end shortening, L is the length of the stub column specimen. It is observed that the stocky sections exhibit superior normalised load-carrying capacity with significantly larger normalised deformations whereas the slender sections feature limited deformation capacity with normalised resistance decreasing as the width to thickness ratio increase. It is anticipated that materials within the slender sections are not fully utilised due to the occurrence of local buckling and the cross-section capacity of those non-slender sections benefit from the strain hardening at large.

Fig. 23 and Fig. 24 plot the load-axial strain curves for the HSS cold-formed IHexHS stub columns of IHex-170×10-2.00 and IHex-150×10-1.70. The initial parts of the curves are also highlighted to demonstrate the distinct structural behaviour under the axial compression with different material property characteristics. As shown in Figs. 23–24, the load-axial strain curves corresponding to the strain gauges distributing near and at the cold-bent corner portion show higher stress levels in comparison to the load achieved from the other strain gauges under the same strain. The load-axial strain curves corresponding to the strain gauge of No. 1, No. 2, No. 6 and No. 7 displays relatively higher load level among the curves which may be principally due to the involvement of higher level of cold-forming effect whereas the curves corresponding to the strain gauge No. 9 and No. 10 for specimen 170×10-2.00 show relatively lower stress level, possibly due to the effect of the welding and its heat affected zone induced material softening. The failure mode of the stub column specimens is characterized with the typical "inward-outward" deformed mode as shown in Fig. 25.

6. Assessments on cross-section classification and cross-section strength

6.1 Assessment on cross-section classification

Note that the current design codes of practice such as EN 1993-1-12 [29], AISC 360-16 [30], AS 4100 [31] and AISI S100-16 [44] do not provide design provisions for the HSS cold-formed IHexHS. Previous studies demonstrate that plate buckling theory for internal compression elements have been successfully applied for octagonal sections [21, 53]. Hence, the specified limits for the internal plate element under compression

specified in structural steel design codes were evaluated and assessed for theirs' applicability to HSS cold-formed IHexHS.

To deal with the cross-section subject to local buckling, cross-section classification is effectively used and specified in the design codes. Four cross-section classes are categorized in Eurocode EN 1993-1-1 [37], while two classes namely, non-slender (corresponding to Class 1–3) and slender sections (Class 4) are stipulated in AISC 360-16 [30] and AS 4100 [31]. To take the differences of the material strengths into account, material related parameters of $\varepsilon_{EC3} = (235/f_y)^{0.5}$, $\varepsilon_{AISC} = (E/f_y)^{0.5}$, and $\varepsilon_{AS4100} = (250/f_y)^{0.5}$ are used in these three codes respectively. Different from these three codes, design standard of AISI S100 [44] and AS/NZS 4600 [54] adopt parameter λ_p as the cross-section slenderness, where $\lambda p = (fy/fcr)0.5$. EN 1993-1-5 [51] specifies the effective width equations applicable to the sections undergoing local buckling, a cross-section slenderness limit of 0.673 is stipulated. It is thereby also assessed and compared. In addition to the design standards, design approaches such as DSM and CSM, which can be applied to arbitrary cross sections without iterated process in determining the effective area of the sections susceptible to local buckling, are also assessed. DSM specifies that cross-section with slenderness limit λ_p greater than 0.776 cannot reach the yield load, whereas limit value of 0.68 is provided by CSM.

To harmonize the comparisons between various design codes, the yield slenderness limit values from design codes and design approaches are standardized by normalized plate slenderness value $\lambda_{lim} = (b/t)(f_y/E)^{0.5}$, the transformed yield slenderness limits are provided in Table 8. Similar yield slenderness limits are provided by EN 1993-1-1, AISC 360-16 and AS 4100 with 1.405, 1.400 and 1.414 respectively. AISI S100-16 and AS/NZS 4600 give smaller yield limit value of 1.280. Though the cross-section slenderness regulated in AISI S100-16 and DSM are the same, different slenderness yield limit is provided by DSM with 1.34. Likewise, the slenderness limits of CSM with $\lambda_p = 0.68$ is transformed to $\lambda_{lim} = 1.29$. The obtained test results were employed to normalize the cross-section yield load Af_y, where f_y is the 0.2% proof strength obtained from the flat coupon taken from the cold-formed sections. The normalized strengths are subsequently plotted against the governing normalized plate slenderness λ_{lim} within the cross-sections in Fig. 26. As shown in Fig. 26, the current codified yield slenderness limits from structural steel design code are not suitable and cannot be extended for their application to HSS cold-formed IHexHS. The intersection of the yield slenderness limits in design codes with the unity are significantly beyond the point where the data points converge to the unity. Similarly, the converted yield slenderness from DSM and CSM also show overly estimated cross-section classification.

6.2 Cross-section strength under compression

As briefly introduced in sub-section of 6.1, the effective width method is used in EN 1993-1-5, ANSI/AISC 360-16, and AS 4100 for cross sections subjected to local buckling failure prior to the attainment of yielding. The original dimension of the side width b (slender member susceptible to local buckling) of the cross-section is reduced to the effective width of b_{eff} resulting in an effective compressive resistance $A_{eff}f_y$, where A_{eff} is the effective area of the section. Similarly, the other two steel design codes also specify the systematic classification and design system to consider the sections experiencing local buckling. Though the effective width concept is used in these three design codes, different equations are used to determine the effective width of the Class 4 or slender plate elements subject to local buckling, as given in Eqs. (14) – (15),

456 $$\frac{b_{\text{eff,EC3}}}{b}=\begin{cases}1 & \text{for } \overline{\lambda_{\text{p}}}\le 0.673\\ \left(1-0.22/\overline{\lambda_{\text{p}}}\right)/\overline{\lambda_{\text{p}}} & \text{for } \overline{\lambda_{\text{p}}}>0.673\end{cases} \quad (14)$$

457 where $\overline{\lambda_{\text{p}}}$ is the plate slenderness specified in accordance with EN 1993-1-5 [51], where k_σ is the buckling
458 factor taken as 4 for internal plate element in compression.

459 $$\overline{\lambda}_{\text{p}}=\frac{b/t}{28.4\varepsilon_{\text{EC3}}\sqrt{k_\sigma}} \quad (15)$$

460 The effective width method specified in design code of ANSI/AISC 360-16 [30] adopts the limiting width to
461 thickness ratio $\lambda_{\text{p,AISC}}$ instead of plate slenderness, which is equal to the flat width (excluding the corner
462 portions) to thickness (b/t). The expressions are given as follows,

463 $$\frac{b_{\text{eff,AISC}}}{b}=\frac{1.38\lambda_{\text{p,AISC}}}{\lambda}-\frac{0.38\lambda_{\text{p,AISC}}{}^2}{\lambda^2} \quad (16)$$

464 The effective width method stipulated in AS 4100 [31] use material related coefficient of $\varepsilon_{\text{AS4100}} = (250/f_{\text{y}})^{0.5}$
465 and width to thickness ratio b/t.

466 $$\frac{b_{\text{eff,AS4100}}}{b}=\frac{35}{b/(t\varepsilon_{\text{AS4100}})} \quad (17)$$

467 In terms of design approach DSM, the sections can attain the yield load when the cross-section slenderness
468 are within the range of $\lambda_{\text{p}} \le 0.776$, whereas cross-section strength were determined using the equations given
469 in Eq. (18).

470 $$N_{\text{DSM}}=\begin{cases}f_{\text{y}}A & \text{for } \lambda_{\text{p}}\le 0.776\\ 1-\frac{0.15}{\lambda_{\text{p}}{}^{0.8}})\frac{1}{\lambda_{\text{p}}{}^{0.8}}f_{\text{y}}A & \text{for } 0.776>\lambda_{\text{p}}\end{cases} \quad (18)$$

471 To assess the strength predictions from CSM against the experimental results, the base curve available for the
472 commonly used tubular sections SHS/RHS were employed in this study. CSM material model for HSS
473 cold-formed steel proposed by Chen et al. [55] was adopted. The base curve for HSS have been evaluated by
474 Lan et al. [56], as given in Eq. (19).

475 $$\begin{cases}\frac{\varepsilon_{\text{csm}}}{\varepsilon_{\text{y}}}=\frac{0.294}{\lambda_{\text{p}}{}^{3.174}}\le\min(15,\frac{C_1\varepsilon_{\text{u}}}{\varepsilon_{\text{y}}}) & \text{for } \lambda_{\text{p}}\le 0.68\\ \frac{\varepsilon_{\text{csm}}}{\varepsilon_{\text{y}}}=(1-\frac{0.219}{\lambda_{\text{p}}{}^{1.014}})\frac{1}{\lambda_{\text{p}}{}^{1.014}} & \text{for } 0.68<\lambda_{\text{p}}\end{cases} \quad (19)$$

476 where ($\varepsilon_{\text{csm}}/\varepsilon_{\text{y}}$) is the deformation capacity, ε_{csm} is the CSM limiting strain, ε_{y} is the yield strain equal to f_{y}/E.
477 To calculate the cross-section strength from CSM, the CSM limiting stress f_{csm} needs to be derived based on
478 CSM strain, as follows in Eq. (20) where E_{s} is Young's modulus, f_{y} is the yield stress, ε_{y} and ε_{u} are the strains
479 at the yield and ultimate stresses, respectively, ε_{sh} is the strain hardening strain defined as the end of the yield
480 plateau after which the strain hardening initiates, $C_1\varepsilon_{\text{u}}$ represents the strain at the intersection point of the
481 third stage of the model and the actual stress-strain curve. Moreover, material coefficient, C_1 used in the
482 material model defining cut-off strain to avoid over-predictions of material strength.

$$f_{csm} = \begin{cases} E_s \varepsilon_{csm} & \text{for } \varepsilon_{csm} \le \varepsilon_y \\ f_y + E_{sh}(\varepsilon_{csm} - \varepsilon_{sh}) & \text{for } \varepsilon_y < \varepsilon_{csm} < C_1 \varepsilon_u \end{cases} \quad (20)$$

The hardening modulus of E_{sh} can be determined according to Eq. (21) with material coefficient C_2.

$$E_{sh} = \frac{f_u - f_y}{C_2 \varepsilon_u - \varepsilon_y} \quad (21)$$

For the relatively compact sections with cross-section slenderness lower than 0.68, the cross-section strength is determined as CSM limiting stress multiplied by gross area A, whereas the deformation capacity of ($\varepsilon_{csm}/\varepsilon_y$) is used for cross-section with slenderness greater than 0.68. The equation of cross-section strength from CSM is as follows in Eq. (22),

$$N_{csm} = \begin{cases} f_{csm} A & \text{for } \lambda_p \le 0.68 \\ \dfrac{\varepsilon_{csm}}{\varepsilon_y} f_y A & \text{for } \lambda_p > 0.68 \end{cases} \quad (22)$$

The test results were normalized with the predicted strength from design codes and design approaches with all partial factors set to unity for direct comparison. The normalized strength ratios are plotted against the corresponding plate slenderness λ_p and compared with effective width equation codified in three structural steel design codes. As shown in Fig. 27, for the compact sections failed by cross-section yielding, all three design codes generate over-conservative predictions due to the neglect of strain hardening. Compared with EN 1993-1-5 and AISC 360-16, strength predicted from AS 4100 provides more reliable results on safe side. Similarly, the design approaches of DSM and CSM also show inappropriate predictions for slender sections experiencing local buckling, as shown in Fig. 28. Key test results with the statistical analysis of the cross-section resistance prediction comparisons, including the mean test-to-predicted compression resistance ratios $N_u/N_{u,pred}$, the corresponding coefficient of variations (CoVs) are shown in Table 7. Table 7 shows that 11 out of 20 specimens are failed by local buckling. The predictions from the design codes are consistent and slightly conservative. The mean values of $N_u/N_{u,pred}$ obtained from design codes of EN 1993-1-12, AISC 360-16, AS4100, AISI S100-16 and design approaches are 1.03, 1.02, 1.05, 1.03, 1.03 and 1.04 with corresponding CoVs of 0.059, 0.067, 0.041, 0.059, 0.060 and 0.034 respectively. The values of the mean test-to-predicted and the corresponding CoVs are also evaluated for specimens failed by local buckling and cross-section yielding separately with statistical analysis results reported in Table 7. The results show that all design codes tend to underestimate the cross-section strength, whereas the cross-section predictions for slender sections are markedly unconservative except for AS 4100 whereas CSM provides conservative predictions. EN 1993-1-12, AISI S100-16 and DSM give close predictions for slender sections, and CSM generate more accurate results for non-slender sections as anticipated since it can account for the materials strain hardening.

7. Conclusions

A total of 20 cold-formed HSS IHexHS stub columns were tested to investigate the local buckling behaviour and the cross-section resistance. Initial local geometric imperfections were measured prior to the compression tests and the material properties were studied by which the predictive strength enhancement

models were assessed and evaluated against the test results from corner coupons. The applicability of the existing design codes and design approaches for HSS cold-formed IHexHS were assessed and compared against the obtained test results. Cross-section strength determined in accordance with the design codes and the design methods were compared with the test results. Based on the experimental study presented in this paper, the following conclusions can be drawn:

(a) The flat coupons and corner coupons generally meet the requirements of the strength ratio f_u/f_y lower than 1.05 as specified in EN 1993-1-12. Almost all coupons except for two coupons meet the requirement of elongation of fracture higher than 10%. The corner coupons cannot meet the requirements of strain at failure due to the press-braking process. Increased strength from corner coupons can be accurately predicted using the proposed predictive model.

(b) The initial local geometric imperfections are practically proportional to the cross-section slenderness and a predictive model of initial local geometric imperfection is proposed.

(c) The current codified yield slenderness limits in structural steel design codes cannot be extended for application to HSS cold-formed IHexHS stub column under pure compression.

(d) Based on current codified yield slenderness limits, all structural steel design codes provide over-conservative predictions for cross-section strength due to the neglect of strain hardening.

(e) Based on current codified yield slenderness limits, compared with EN 1993-1-12 and AISC 360-16, strength predicted from AS 4100 provides more reliable results on safe side for slender sections. Though the design approaches of DSM and CSM show inappropriate predictions for slender sections experiencing local buckling, CSM yield more accurate results for compact sections.

Data Availability Statement

Some or all data that support the findings of this study are available from the corresponding author upon reasonable request.

Acknowledgement

The research work presented in this paper was supported by a grant from the Research Grants Council of the Hong Kong Special Administrative Region, China (Project no. 15218918). The authors would also like to thank the technical staff, Mr. H.Y. Leung, Mr. K.H. Wong, Mr. K.L. Cheung of the Structural Engineering Research Laboratory for their support as well as the support from the Industrial Center at The Hong Kong Polytechnic University.

References

[1] Bjorhovde R. Development and use of high performance steel. J Constr Steel Res. 2004;60:393-400.
[2] Liu JZ, Fang H, Chen S, Chan T-M. Material properties and residual stresses of high strength steel hexagonal hollow sections. J Constr Steel Res. 2022;190:107061.

563 [3] Shi G, Hu FX, Shi YJ. Recent research advances of high strength steel structures and codification of
564 design specification in China. Int J Steel Struct. 2014;14:4:873-887.
565 [4] Tseung Kwan O Bridge in Hong Kong [Image], Available from: https://www.cbltko.hk/en/news.php,
566 2019.
567 [5] Liu JZ, Fang H, Chan TM. Experimental investigation on material properties and residual stresses in
568 cold-formed high strength steel irregular octagonal hollow sections. J Constr Steel Res. 2022;191:107170.
569 [6] Meng X, Gardner L. Testing of hot-finished high strength steel SHS and RHS under combined
570 compression and bending. Thin-Walled Struct. 2020;148:106262.
571 [7] Usami T, Fukumoto Y. Local and overall buckling of welded box columns. J Struct Div.
572 1982;108:525-42.
573 [8] Rasmussen KJ, Hancock GJ. Plate slenderness limits for high strength steel sections. J Constr Steel Res.
574 1992;23:73-96.
575 [9] Clarin M. High strength steel: local buckling and residual stresses: Luleå tekniska universitet; 2004.
576 [10] Gao L, Sun H, Jin F, Fan H. Load-carrying capacity of high-strength steel box-sections I: Stub columns.
577 J Constr Steel Res. 2009;65:918-24.
578 [11] Kim D-K, Lee C-H, Han K-H, Kim J-H, Lee S-E, Sim H-B. Strength and residual stress evaluation of
579 stub columns fabricated from 800MPa high-strength steel. J Constr Steel Res. 2014;102:111-20.
580 [12] Shi G, Zhou W, Bai Y, Lin C. Local buckling of 460 MPa high strength steel welded section stub
581 columns under axial compression. J Constr Steel Res. 2014;100:60-70.
582 [13] Schillo N, Feldmann M. Local buckling behaviour of welded box sections made of high-strength steel.
583 Steel Construction. 2015;8:179-86.
584 [14] Schillo N, Feldmann M. Interaction of local and global buckling of box sections made of high strength
585 steel. Thin-Walled Struct. 2018;128:126-40.
586 [15] Wang J, Afshan S, Schillo N, Theofanous M, Feldmann M, Gardner L. Material properties and
587 compressive local buckling response of high strength steel square and rectangular hollow sections. Eng Struc.
588 2017;130:297-315.
589 [16] Gkantou M, Theofanous M, Antoniou N, Baniotopoulos C. Compressive behaviour of high-strength
590 steel cross-sections. Proceedings of the Institution of Civil Engineers. 2017;170:813-24.
591 [17] Zhao XL. Section capacity of very high strength (VHS) circular tubes under compression. Thin-Walled
592 Struct. 2000;37:223-40.
593 [18] Jiao H, Zhao XL. Imperfection, residual stress and yield slenderness limit of very high strength (VHS)
594 circular steel tubes. J Constr Steel Res. 2003;59:233-49.
595 [19] Ma J-L, Chan T-M, Young B. Experimental Investigation on Stub-Column Behavior of Cold-Formed
596 High-Strength Steel Tubular Sections. J Struct Eng. 2016;142:04015174.
597 [20] Meng X, Gardner L. Cross-sectional behaviour of cold-formed high strength steel circular hollow
598 sections. Thin-Walled Struct. 2020;156:106822.
599 [21] Fang H, Chan T-M, Young B. Behavior of Octagonal High-Strength Steel Tubular Stub Columns. J
600 Struct Eng. 2019;145. 04019150.
601 [22] Fang H, Chan T-M, Young B. Experimental and Numerical Investigations of Octagonal High-Strength
602 Steel Tubular Stub Columns under Combined Compression and Bending. J Struct Eng. 2021;147:04020282.
603 [23] Fang H, Chan T-M, Young B. Structural performance of concrete-filled cold-formed high-strength steel
604 octagonal tubular stub columns. Eng Struc. 2021;239:112360.
605 [24] Chen JB, Liu HX, Chan TM. Material properties and residual stresses of cold-formed octagonal hollow
606 sections. J Constr Steel Res. 2020;170.

[25] Chen J, Fang H, Chan T-M. Design of fixed-ended octagonal shaped steel hollow sections in compression. Eng Struc. 2021;228:111520.
[26] Dalia ZM, Bhowmick AK, Grondin GY. Local buckling of multi-sided steel tube sections under axial compression and bending. J Constr Steel Res. 2021;186:106909.
[27] Xu W, Han L-H, Li W. Performance of hexagonal CFST members under axial compression and bending. J Constr Steel Res. 2016;123:162-75.
[28] Liu J-Z, Fang H, Chan T-M. Investigations on material properties and residual stresses in cold-formed high strength steel irregular hexagonal hollow sections. Thin-Walled Struct. 2022; 175: 109220.
[29] EN 1993-1-12, Eurocode 3: Design of Steel Structures – Part 1–12: Additional Rules for the Extension of EN 1993 up to Steel Grades S700. Brussels: European Committee for Standardization (CEN); 2007.
[30] ANSI/AISC 360-16, Specification for Structural Steel Buildings. Chicago: American Institute of Steel Construction (AISC); 2016.
[31] AS 4100-1998(R2016), Steel structures (Reconfirmed 2016 Incorporating Amendment No.1), AS 4100. Sydney, Australia: Australian Standard; 2016.
[32] Schafer BW. Review: The Direct Strength Method of cold-formed steel member design. J Constr Steel Res. 2008;64:766-78.
[33] Gardner L, Nethercot DA. Structural stainless steel design: A new approach. Structural Engineer. 2004;82:21-8.
[34] EN 10219-2, Cold formed welded steel structural hollow sections. Tolerances, dimensions and sectional properties. Brussels: European Committee for Standardization (CEN); 2019.
[35] AWS A5.28/A5.28M, Specification for Low-Alloy Steel Electrodes and Rods for Gas Shielded Arc Welding. United States of America: American Welding Society; 2005.
[36] EN ISO 6892-1, Metallic Materials – Tensile Testing Part 1: Method of Test at Ambient Temperature. EN ISO 6892-1. Brussels, Belgium: CEN; 2019.
[37] EN 1993-1-1, Eurocode 3: Design of Steel STRUCTURES – Part 1.1: General Rules and Rules for Buildings. Brussels: European Committee for Standardization (CEN); 2005.
[38] National Annex to Eurocode 3: Design of steel structures - Part 1-1: General rules and rules for buildings. UK National Annex to EN 1993-1-1, 2015. BS; 2015.
[39] National Annex to Eurocode 3: Design of steel structures - Part 1-12: Additional rules for the extension of EN 1993 up to steel grades S 700. UK National Annex to EN 1993-1-12, 2008. BS; 2008.
[40] Yuhshi, Fukumoto. New constructional steels and structural stability. Eng Struc. 1996;18:786-91.
[41] Langenberg P. Relation between design safety and Y/T ratio in application of welded high strength structural steels. International Symposium on Application of High Strength Steels in Modern Constructions and Bridges-Relationship of Design Specification, Safety and Y/T Ratio. Beijing, China2008. p. 28-46.
[42] Gardner L, Yun X. Description of stress-strain curves for cold-formed steels. Constr Build Mater. 2018;189:527-38.
[43] Karren KW. Corner properties of cold-formed steel shapes. J Struct Div. 1967;93:401-32.
[44] AISI S100-16, North American Specification for the Design of Cold-Formed Steel Structural Members. Washington, DC, USA: AISI (American Iron and Steel Institute); 2016.
[45] Pham CH, Trinh HN, Proust G. Effect of manufacturing process on microstructures and mechanical properties, and design of cold-formed G450 steel channels. Thin-Walled Struct. 2021;162:107620.
[46] Gardner L, Saari N, Wang F. Comparative experimental study of hot-rolled and cold-formed rectangular hollow sections. Thin-Walled Struct. 2010;48:495-507.
[47] Schafer B, Peköz T. Computational modeling of cold-formed steel: characterizing geometric

651 imperfections and residual stresses. J Constr Steel Res. 1998;47:193-210.
652 [48] Chen J, Chan T-M, Varma AH. Stub Column Behavior of Cold-Formed High-Strength Steel Circular
653 Hollow Sections under Compression. J Struct Eng. 2020;146:04020277.
654 [49] Liu JZ, Chen S, Chan TM, Testing, numerical modelling and design of Q690 high strength steel welded
655 T-section stub columns. Eng Struc. 2022; 259:114142.
656 [50] Liu JZ, Chen S, Chan TM, Experimental and numerical investigations of hybrid high strength steel
657 welded T-section stub columns with Q690 flange and Q460 web. Thin-Walled Struc. 2022; (xxx): 109403.
658 (in publication).
659 [51] EN 1993-1-5, Eurocode 3: Design of Steel Structures – Part 1–5: Plated structural elements. Brussels:
660 European Committee for Standardization (CEN); 2006.
661 [52] Dawson RG, Walker AC. Post-Buckling of Geometrically Imperfect Plates. J Struct Div. 1972;98:75-94.
662 [53] Zhu JY, Chan TM, Young B. Cross-sectional capacity of octagonal tubular steel stub columns under
663 uniaxial compression. Eng Struc. 2019;184:480-94.
664 [54] AS/NZS 4600:2018, Cold-formed steel structures, AS/NZS 4600. Sydney, Australia and Wellington,
665 New Zealand: Australian/New Zealand Standards; 2018.
666 [55] Chen S, Fang H, Liu J-z, Chan T-M. Design for local buckling behaviour of welded high strength steel
667 I-sections under bending. Thin-Walled Struct. 2022;172:108792.
668 [56] Lan XY, Chen JB, Chan TM, Young B. The continuous strength method for the design of high strength
669 steel tubular sections in compression. Eng Struc. 2018;162:177-87.

(a)

(b)

Fig. 1. Typical engineering applications of HSS (a) Phoenix International Media Center [3] (b) Tseung Kwan O bridge [4]

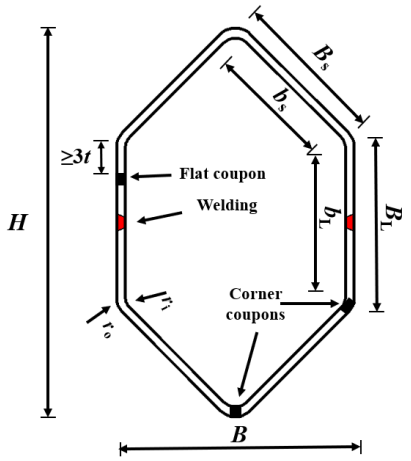

Fig. 2. Cross section of the HSS cold-formed irregular hexagonal hollow section.

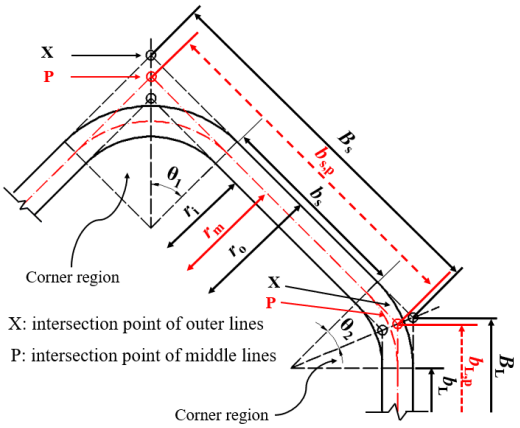

Fig. 3. Detailed geometry and symbol definitions of the HSS cold-formed irregular hexagonal hollow section.

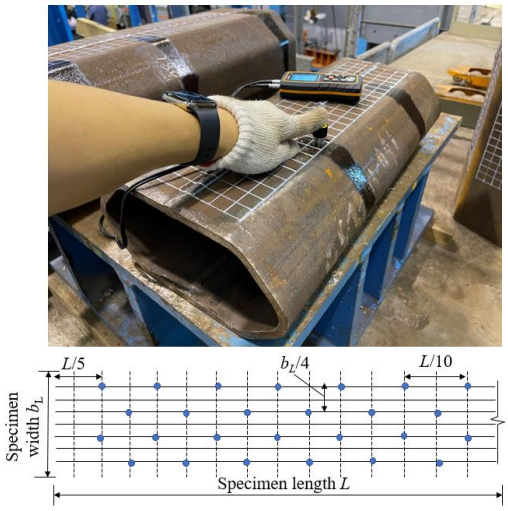

Fig. 4. Measurements of the thickness of HSS cold-formed irregular hexagonal hollow section.

(a)

(b)

Fig. 5. Test set-up for tensile coupon tests (a) Test set-up for flat coupon specimen (b) Test set-up for corner coupon specimen.

(a) Flat coupons from the sections

(b) Corner coupons from the sections

Fig. 6. Failed tensile coupon specimens taken from the HSS cold-formed irregular hexagonal hollow sections.

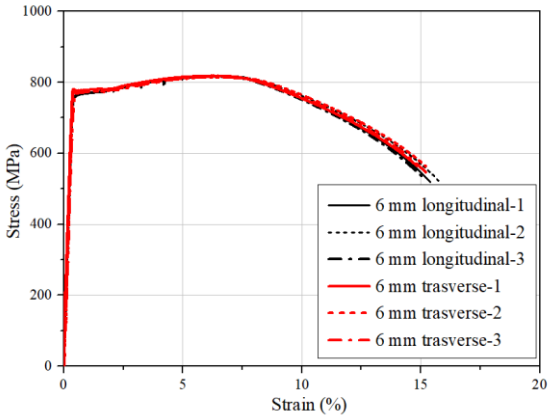

Fig. 7. Measured material stress-strain curves of Q690 high strength steel longitudinal and transverse tensile coupons extracted from 6 mm thick parent plate.

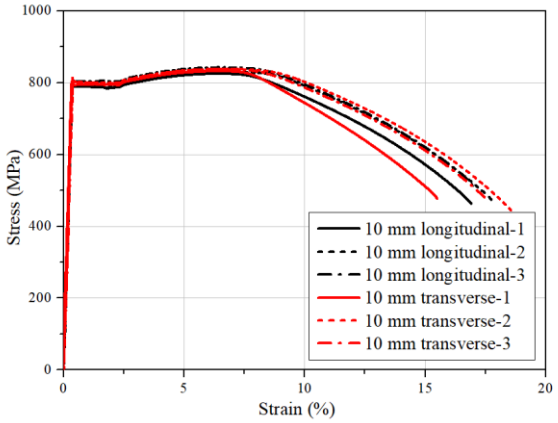

Fig. 8. Measured material stress-strain curves of Q690 high strength steel longitudinal and transverse tensile coupons extracted from 10 mm thick parent plate

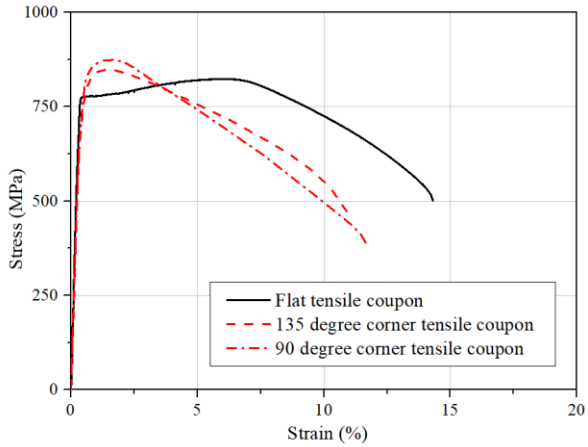

Fig. 9. Typical measured material stress-strain curves of tensile coupons extracted from HSS cold-formed IHexHS stub column of IHex-125×6-1.60.

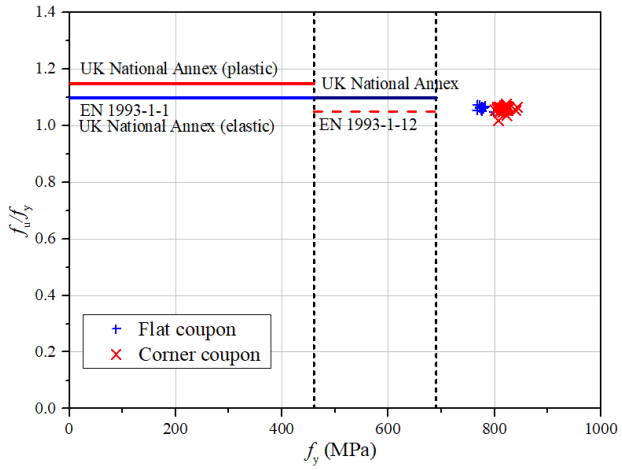

Fig. 10. Requirements on the ratio between yield strength and ultimate strength.

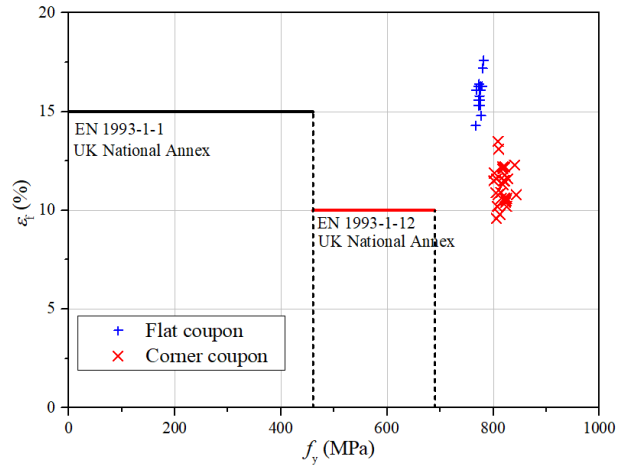

Fig. 11. Requirements on the elongation at facture.

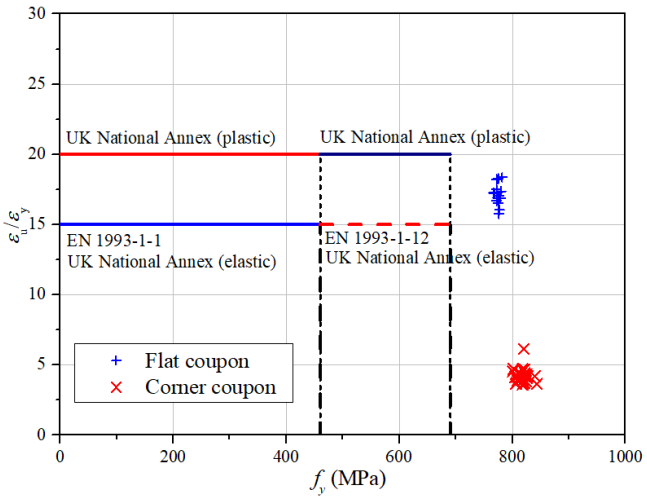

Fig. 12. Requirements on the ratio between ultimate strain and yield strain.

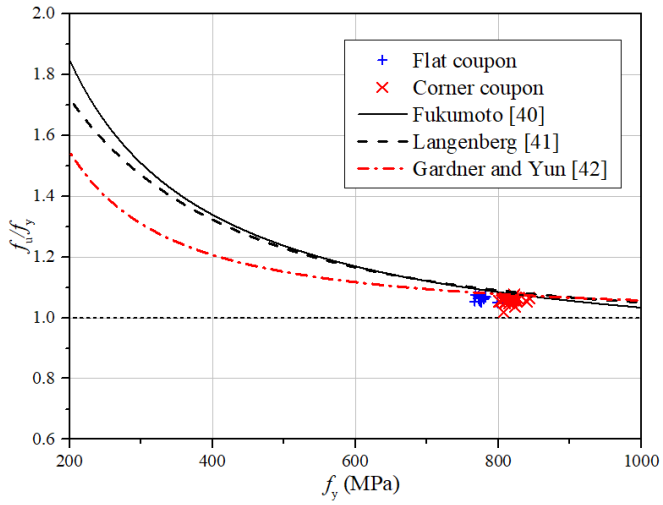

Fig. 13. Assessment of the variation of f_u/f_y with yield strength f_y for both flat and corner coupons.

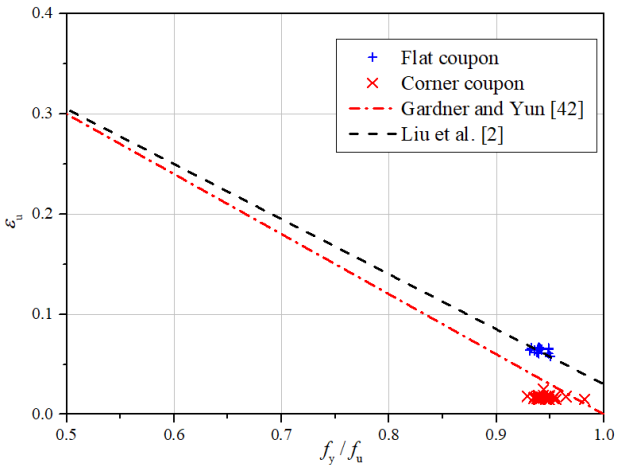

Fig. 14. Assessment of the variation of ε_u with for both flat and corner coupons taken from HSS cold-formed IHexHS.

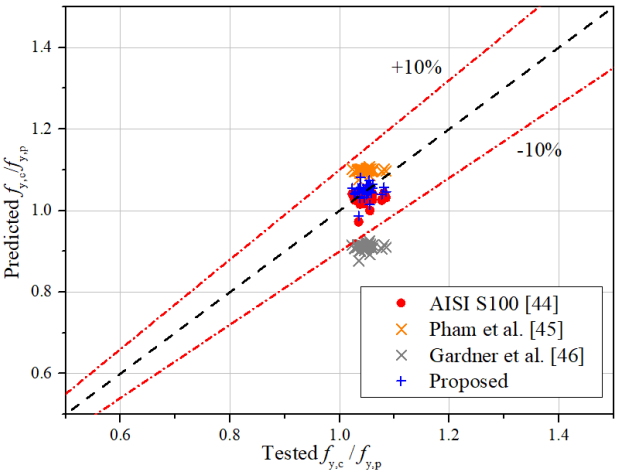

Fig. 15. Assessment of the strength enhancement predictive models.

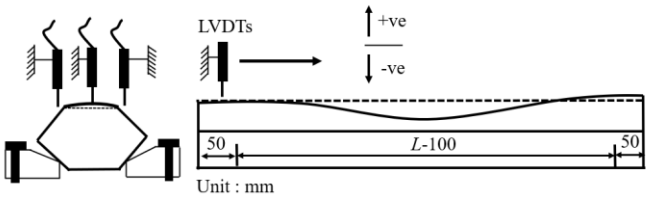

(a) Schematic view

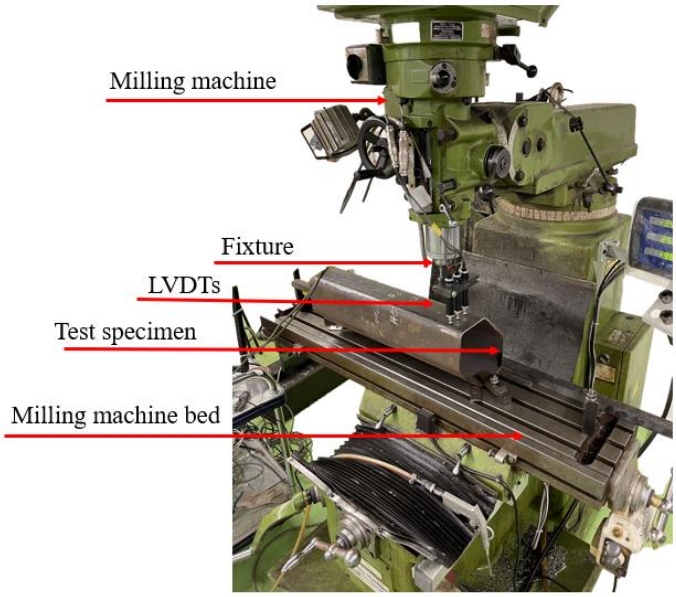

(b) Experimental arrangement

Fig. 16. Set-up of the local geometric imperfection measurement for HSS IHexHS stub column

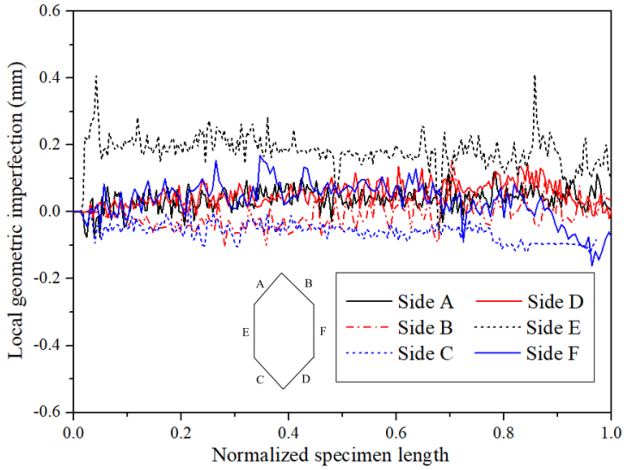

Fig. 17. The distribution of local geometric imperfections along the length of IHexHS stub column specimen IHex-160×6-1.90.

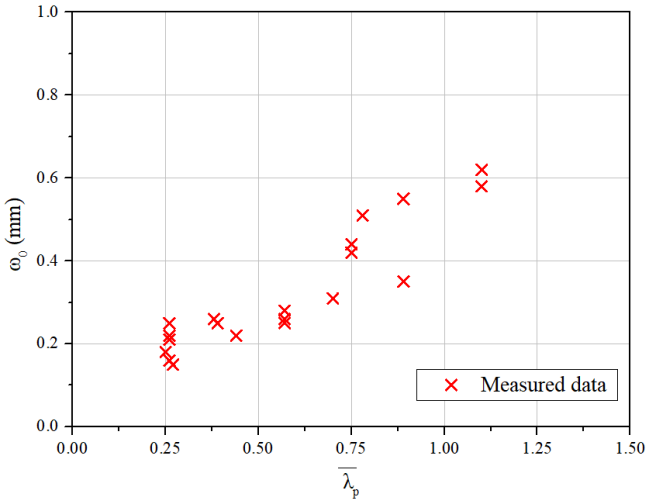

(a)

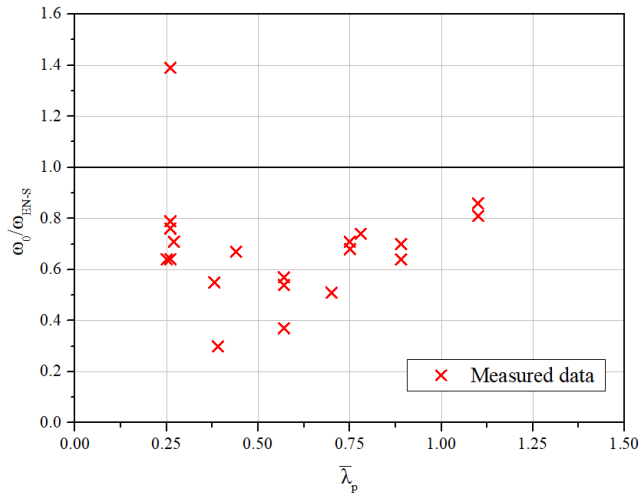

(b)

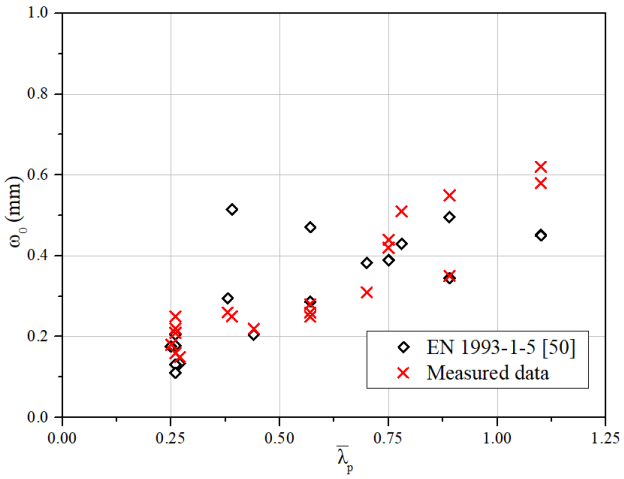

(c)

Fig. 18. Variation of the measured initial local geometric imperfections with plate slenderness (a) imperfection amplitude (b) comparison with fabrication requirement of EN 10219 (c) comparison with the initial imperfection set out in EN 1993-1-5 for plate elements.

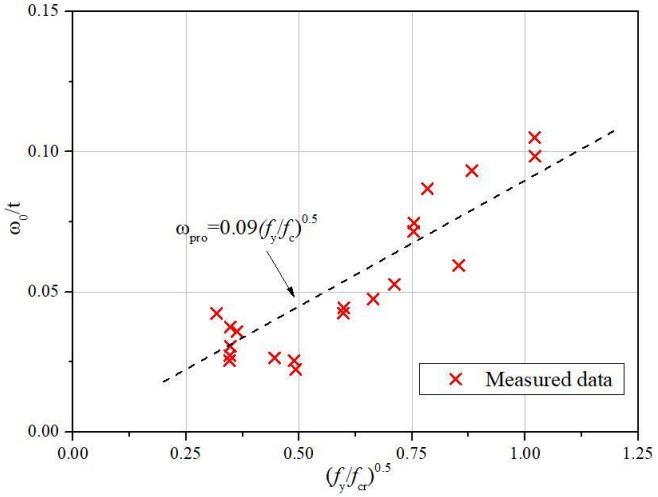

Fig. 19. Comparison of the measured initial imperfection with the proposed imperfection predictive model for HSS cold-formed IHexHS

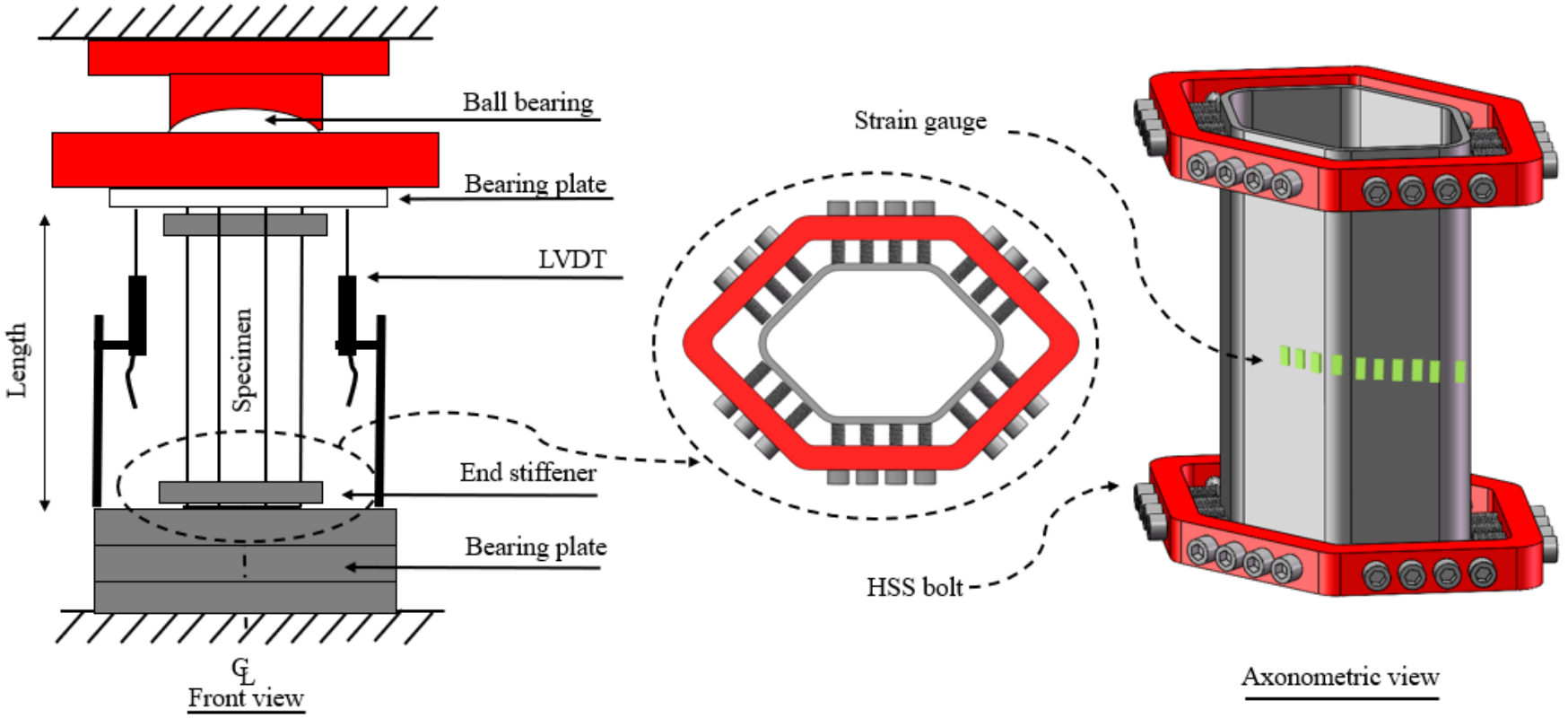

(a) Schematic view of the test set-up and the end stiffeners

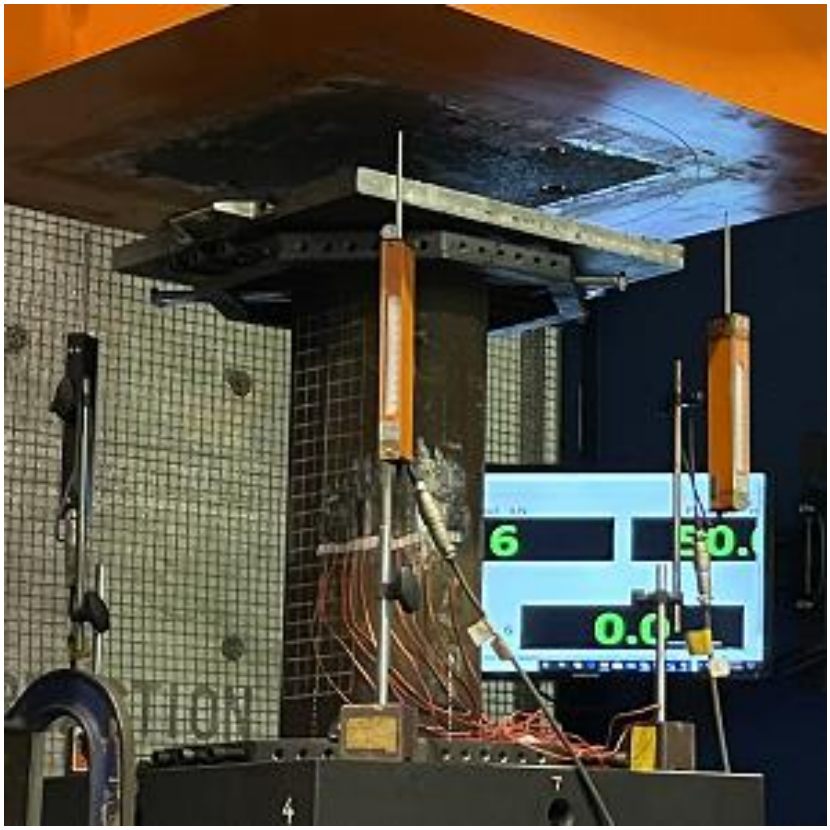

(b) Experimental arrangement

Fig. 20. Test set-up for HSS cold-formed IHexHS stub column under concentric compression

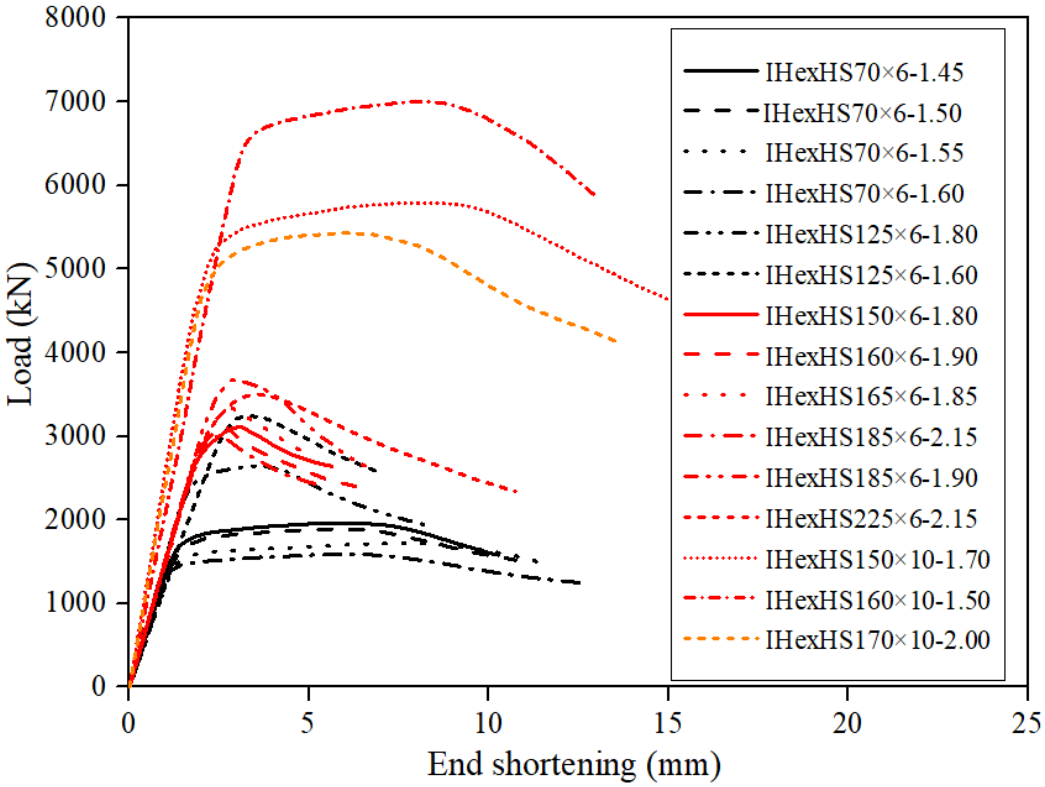

Fig. 21. Load-end shortening curves of the cold-formed HSS IHextHS stub columns.

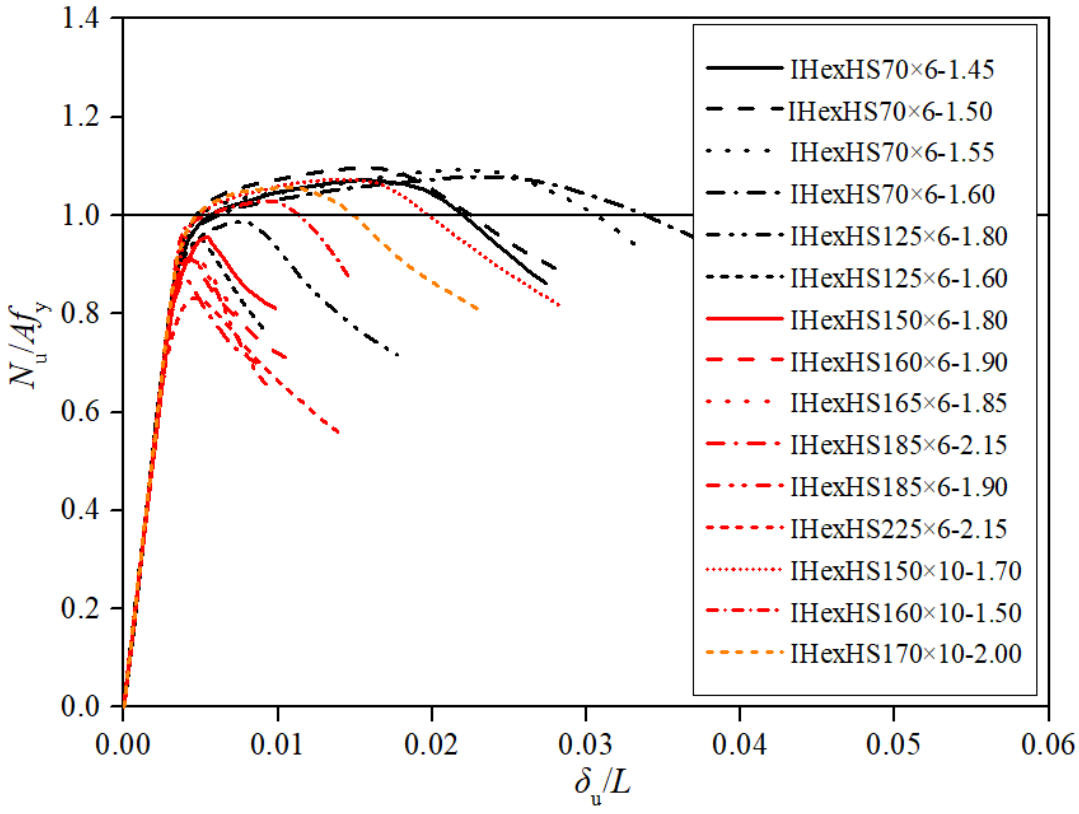

Fig. 22. Normalized load-end shortening curves of the cold-formed HSS IHexHS stub columns

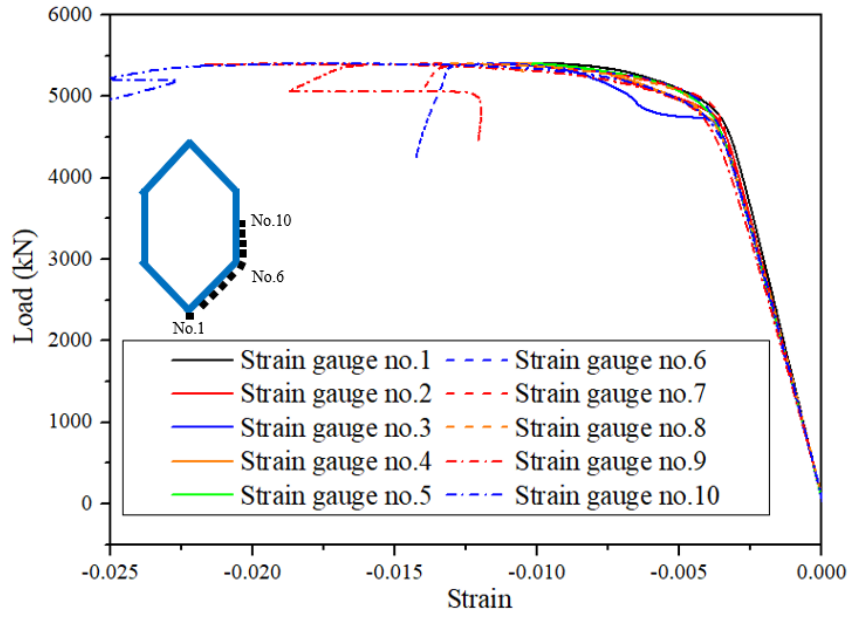

(a)

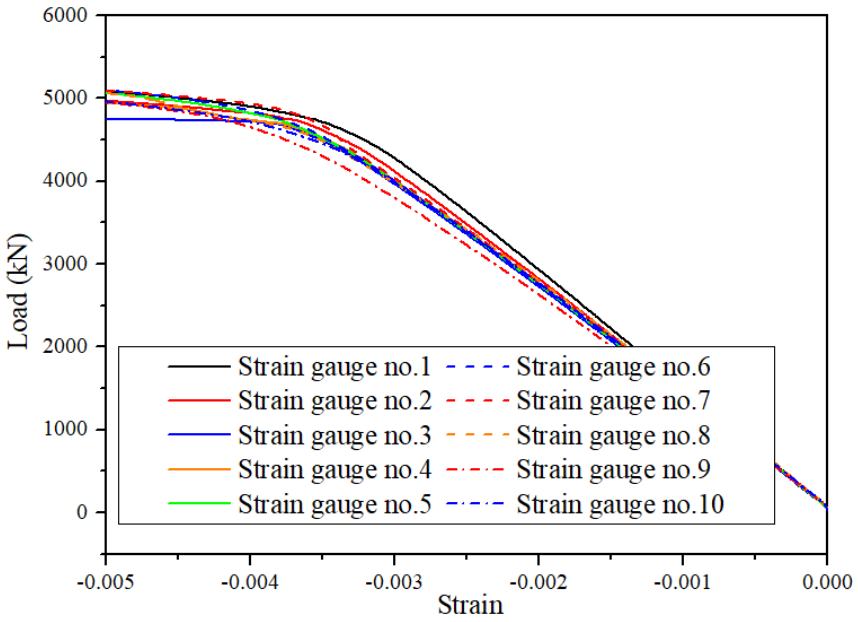

(b)

Fig. 23. Comparison of load-strain relationship of HSS IHextHS stub column specimen IHex-170×10-2.00 (a) Complete load-strain curves (b) Initial part of load-strain curves

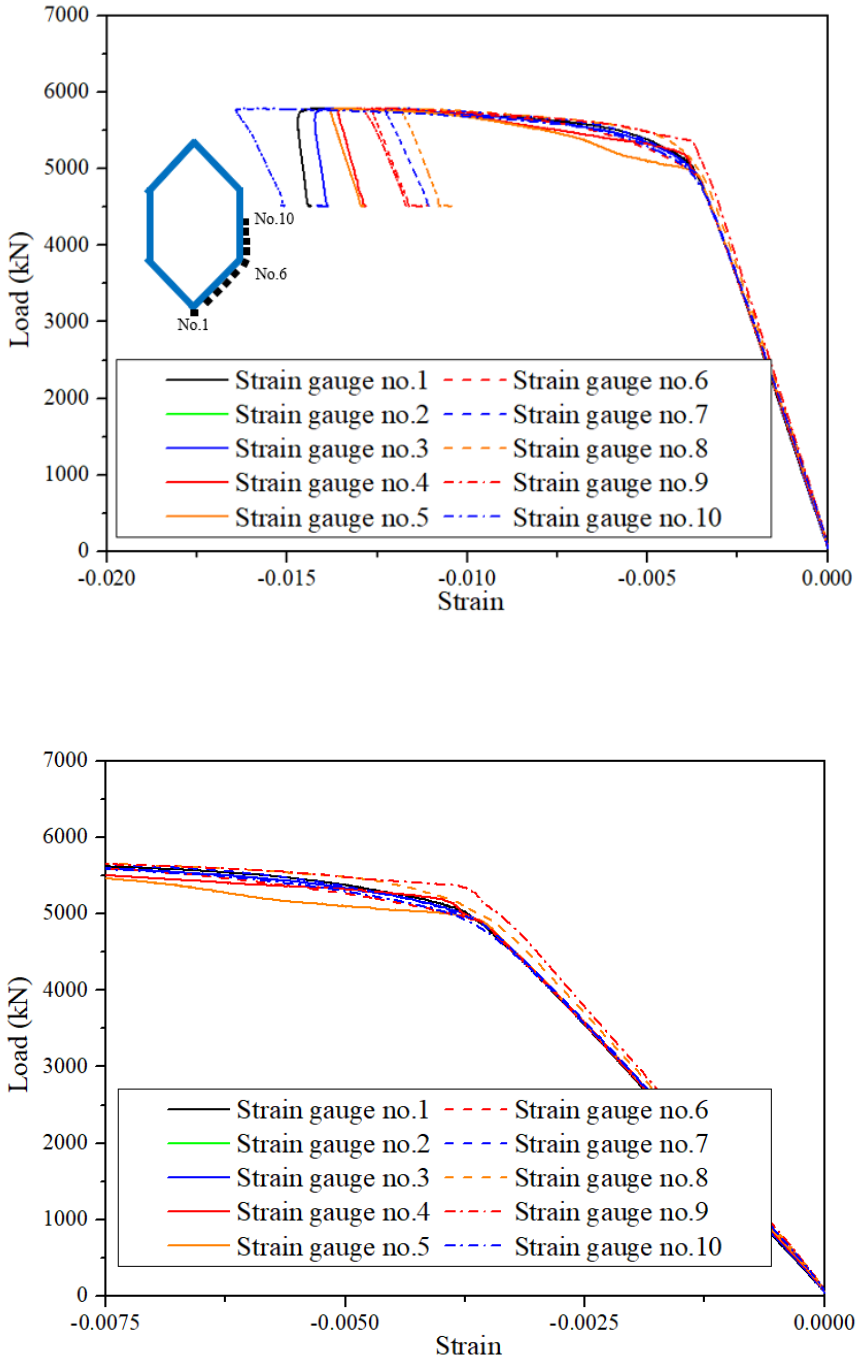

Fig. 24. Comparison of load-strain relationship of HSS IHextHS stub column specimen IHex-150×10-1.70 (a) Complete load-strain curves (b) Initial part of load-strain curves

Fig. 25. Experimental failure modes of the representative cold-formed HSS IHextHS stub columns

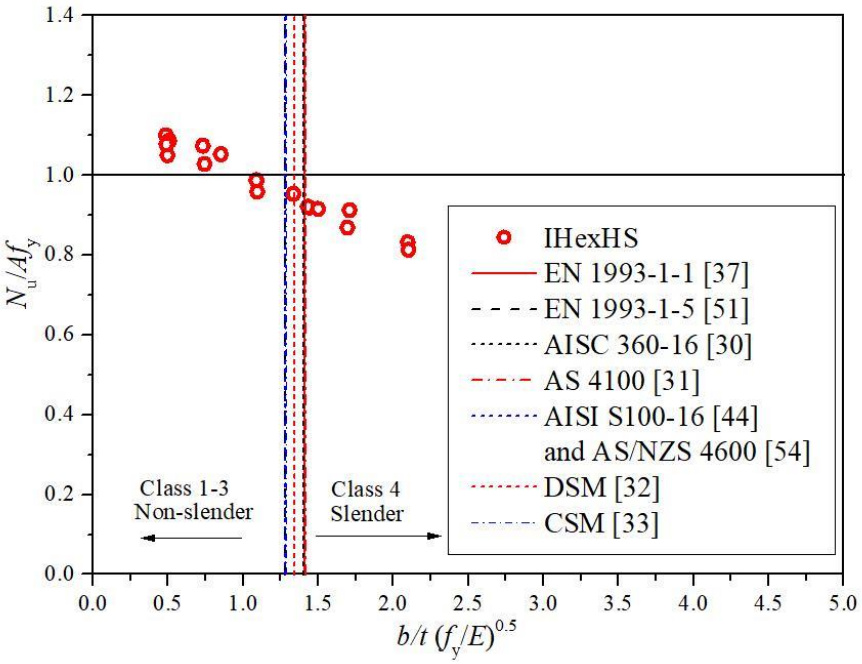

Fig. 26. Assessment of slenderness limits in the design codes and design approaches for HSS cold-formed IHexHS stub column in compression.

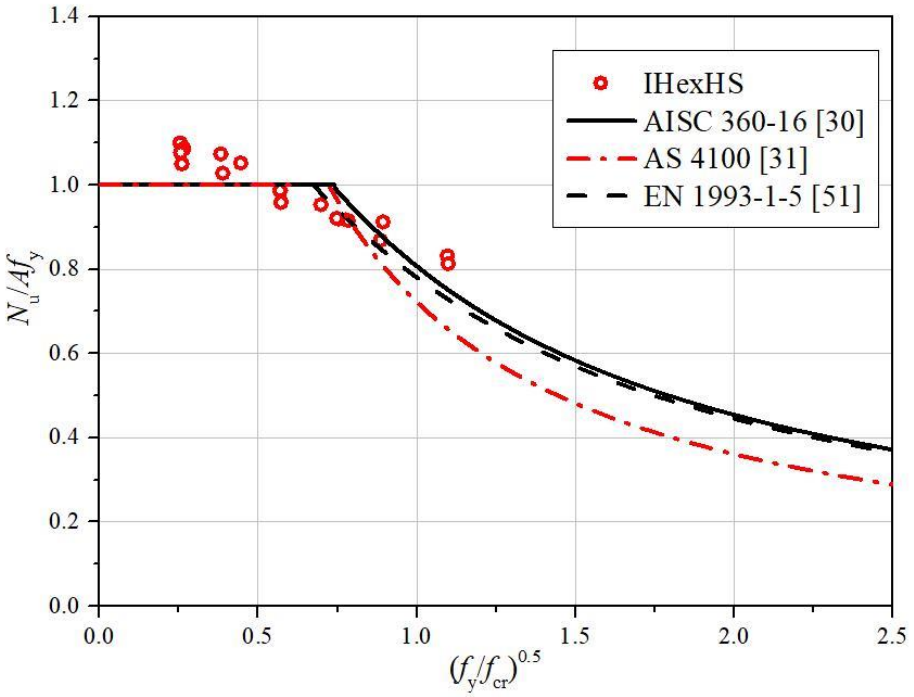

Fig. 27. Assessment of the effective width methods in design codes for HSS cold-formed IHexHS stub column in compression.

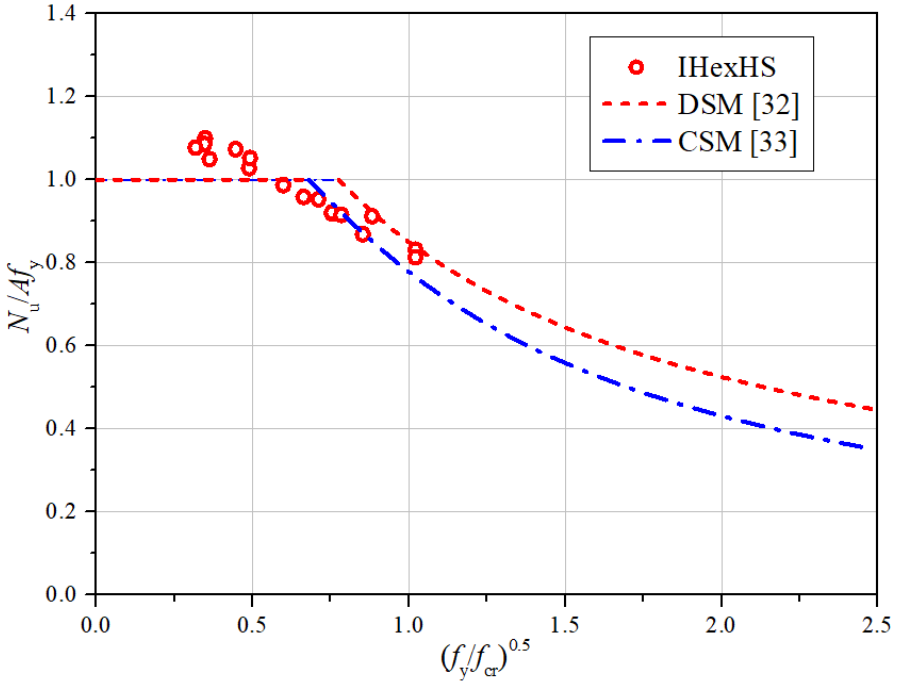

Fig. 28. Assessment of the design approaches DSM and CSM for HSS cold-formed IHexHS stub column in compression.

Table 1 Dimensions of the HSS irregular hexagonal stub column sections.

Section	Edge length B_s (mm)	Side width b_s (mm)	Edge length B_L (mm)	Side width b_L (mm)	Section depth H (mm)	Thickness t (mm)	Length L (mm)	Inner radius r_i (mm)	b_s/t (-)	b_L/t (-)	Area A (mm^2)
IHex-70×6-1.45	74.9	41	67.6	47.7	153.7	5.86	375	18.0	6.9	8.1	2348.4
IHex-70×6-1.50	69.5	35.6	66.9	47.0	145.4	5.87	375	18.0	6.1	8.0	2210.1
IHex-70×6-1.50#	69.2	35.2	66.6	46.8	145.2	5.88	375	18.0	6.0	8.0	2208.2
IHex-70×6-1.55	60.6	26.7	68.8	48.9	134.7	5.87	348	18.0	4.5	8.3	2019.3
IHex-70×6-1.55#	60.3	26.2	68.5	48.5	134.3	5.86	348	18.0	4.5	8.3	2019.1
IHex-70×6-1.60	56.0	22.1	67.2	47.3	126.6	5.90	260	18.0	3.7	8.0	1889.7
IHex-125×6-1.80	91.4	57.5	125.1	105.2	234.5	5.88	475	18.0	9.8	17.9	3434.1
IHex-125×6-1.80#	91.2	57.4	125.0	105.1	234.4	5.89	475	18.0	9.7	17.8	3433.5
IHex-125×6-1.60	128.1	94.2	125.7	105.9	287.1	5.90	750	18.0	15.9	17.9	4322.7
IHex-150×6-1.80	110.4	76.5	148.6	128.8	284.9	5.88	575	18.0	13.0	21.9	4172.7
IHex-160×6-1.90	111.9	78.0	158.6	138.7	297.0	5.87	600	18.0	13.3	23.6	4328.1
IHex-160×6-1.90#	111.5	77.8	158.1	138.5	296.8	5.90	600	18.0	13.2	23.4	4327.9
IHex-165×6-1.85	120.0	86.0	164.3	144.4	314.0	5.87	635	18.0	14.7	24.6	4588.5
IHex-185×6-2.15	102.9	69.0	183.4	163.5	309.1	5.88	625	18.0	11.7	27.8	4409.7
IHex-185×6-1.90	133.1	99.2	185.4	165.5	353.8	5.90	715	18.0	16.8	28.1	5158.5
IHex-225×6-2.15	124.2	90.3	222.9	203.0	378.7	5.90	765	18.0	15.3	34.4	5394.4
IHex-225×6-2.15#	124.0	90.1	222.6	203.1	378.8	5.89	765	18.0	15.3	34.5	5392.2
IHex-150×10-1.70	115.6	59.0	151.1	118.0	281.4	9.83	575	30.0	6.0	12.0	6919.1
IHex-160×10-1.50	159.6	103.0	153.1	120.0	345.7	9.84	875	30.0	10.5	12.2	8719.1
IHex-170×10-2.00	97.6	41.0	170.3	137.2	275.2	9.82	585	30.0	4.2	14.0	6583.1

Note: # indicates the repeated test

Table 2 Mean test results of the flat coupon specimens taken from the HSS parent plates.

Section	$E_{s,p}$ (GPa)	v	$f_{y,p}$ (Mpa)	$f_{u,p}$ (Mpa)	$\varepsilon_{u,p}$ (%)	$\varepsilon_{f,p}$ (%)	$\varepsilon_{sh,p}$ (%)
6 mm plate	214.1	0.29	768.5	816.2	6.45	14.95	1.98
10 mm plate	216.1	0.30	791.3	825.6	6.55	16.18	2.32

Table 3 Test results of the material properties of the flat coupon specimens taken from the sections.

Section	E_s (GPa)	f_y (MPa)	f_u (MPa)	ε_u (%)	$\varepsilon_{f,ex}$ (%)	ε_f (%)	$f_{0.05}$ (MPa)
IHex-70×6-1.45	217.1	767	809	6.1	14.3	15.1	767
IHex-70×6-1.50	203.5	776	818	6.5	16.1	15.8	769
IHex-70×6-1.55	211.2	772	822	6.1	15.6	15.3	772
IHex-70×6-1.60	198.1	774	816	6.6	15.8	16.2	771
IHex-125×6-1.80	206.5	768	825	6.4	16.1	16.4	774
IHex-125×6-1.60	205.1	773	824	6.5	16.4	16.1	770
IHex-150×6-1.80	204.6	772	821	6.6	16.3	15.6	765
IHex-160×6-1.90	211.2	775	825	6.7	15.6	15.2	771
IHex-165×6-1.85	201.2	777	829	6.2	14.8	15.5	772
IHex-185×6-2.15	224.4	782	836	6.4	17.6	18.1	773
IHex-185×6-1.90	213.1	772	828	6.6	15.3	15.1	765
IHex-225×6-2.15	211.7	780	831	6.4	17.2	17.6	774
IHex-150×10-1.70	211.1	776	817	5.8	16.3	16.8	775
IHex-160×10-1.50	206.5	775	826	6.2	15.3	15.2	770
IHex-170×10-2.00	202.6	779	827	6.5	16.3	15.8	768

Table 4 Test results of the material properties of the corner coupon specimens taken from the sections.

Section	$E_{s,c}$ (GPa)	$f_{y,c}$ (MPa)	$f_{u,c}$ (MPa)	$\varepsilon_{u,c}$ (%)	$\varepsilon_{f,ex,c}$ (%)	$\varepsilon_{f,c}$ (%)	$f_{0.05,c}$ (MPa)
IHex-70×6-1.45-90	197.7	825	871	1.7	10.6	11.5	761
IHex-70×6-1.45-135	198.6	823	853	1.8	10.4	11.2	758
IHex-70×6-1.50-90	195.4	818	862	1.5	11.3	10.9	721
IHex-70×6-1.50-135	197.3	815	854	1.8	10.6	10.3	730
IHex-70×6-1.55-90	195.6	806	858	1.5	9.6	10.5	677
IHex-70×6-1.55-135	199.8	807	822	1.5	10.2	10.7	766
IHex-70×6-1.60-90	193.7	812	857	1.7	9.8	10.1	672
IHex-70×6-1.60-135	201.3	820	869	2.5	11.5	10.6	760
IHex-125×6-1.80-90	200.2	814	865	1.6	10.9	10.5	720
IHex-125×6-1.80-135	198.3	806	856	1.7	11.6	10.9	727
IHex-125×6-1.60-90	199.9	819	872	1.5	10.5	10.9	735
IHex-125×6-1.60-135	209.3	808	860	1.6	10.2	9.5	731
IHex-150×6-1.80-90	192.2	843	898	1.6	10.8	11.8	772
IHex-150×6-1.80-135	195.6	840	885	1.8	12.3	14.2	778
IHex-160×6-1.90-90	202.7	821	868	1.5	11.5	10.7	743
IHex-160×6-1.90-135	208.3	809	847	1.5	10.8	11.2	650
IHex-165×6-1.85-90	208.7	805	851	1.6	10.9	10.5	662
IHex-165×6-1.85-135	201.3	801	845	1.8	11.5	11.2	732
IHex-185×6-2.15-90	203.5	827	880	1.7	11.6	11.9	745
IHex-185×6-2.15-135	202.0	818	871	1.9	12.1	11.6	660
IHex-185×6-1.90-90	201.5	822	885	1.8	12.2	11.8	733
IHex-185×6-1.90-135	198.5	819	876	1.6	11.5	11.2	742
IHex-225×6-2.15-90	196.2	818	868	1.7	12.2	13.5	759
IHex-225×6-2.15-135	195.6	809	849	1.6	13.5	13.2	741
IHex-150×10-1.70-90	198.8	802	845	1.9	11.9	12.5	743
IHex-150×10-1.70-135	199.5	810	863	1.8	13.1	14.8	757
IHex-160×10-1.50-90	197.5	824	879	1.6	10.5	10.8	738
IHex-160×10-1.50-135	203.5	821	878	1.7	10.6	11.2	742
IHex-170×10-2.00-90	198.5	825	872	1.8	10.2	10.6	735
IHex-170×10-2.00-135	202.4	822	871	1.9	11.8	12.6	726

Table 5 Measured material properties from corner coupon specimens and the predicted values using different methods.

Specimen	Experimental results			AISI [44]		Pham et al. [45]		Gardner et al. [46]		Proposed	
	f_y (MPa)	f_u (MPa)	$\frac{f_u}{f_y}$	$f_{y,c,AISI}$ (MPa)	$\frac{f_{y,c,AISI}}{f_y}$	$f_{y,c,Pham}$ (MPa)	$\frac{f_{y,c,Pham}}{f_y}$	$f_{y,c,Gardner}$ (MPa)	$\frac{f_{y,c,Gardner}}{f_y}$	$f_{y,c,pro}$ (MPa)	$\frac{f_{y,c,pro}}{f_y}$
				Eq. (4), (5), (6)		Eq. (4), (7), (8)		Eq. (4), (9), (10)		Eq. (4), (11), (12)	
IHex-70×6-1.45-90	825	871	1.06	802	0.97	855	1.04	708	1.06	814	0.99
IHex-70×6-1.45-135	823	853	1.04	780	0.95	847	1.03	696	1.06	791	0.96
IHex-70×6-1.50-90	818	862	1.05	800	0.98	854	4.04	707	1.05	811	0.99
IHex-70×6-1.50-135	815	854	1.05	793	0.97	852	1.05	703	1.04	804	0.99
IHex-70×6-1.55-90	806	858	1.06	812	1.01	859	1.07	714	1.03	824	1.02
IHex-70×6-1.55-135	807	822	1.02	759	0.94	839	1.04	684	1.03	770	0.95
IHex-70×6-1.60-90	812	857	1.06	802	0.99	855	1.05	708	1.04	813	1.00
IHex-70×6-1.60-135	820	869	1.06	807	0.98	857	1.04	711	1.05	818	1.00
IHex-125×6-1.80-90	814	865	1.06	810	1.00	858	1.05	713	1.04	822	1.01
IHex-125×6-1.80-135	806	856	1.06	810	1.00	858	1.06	712	1.03	821	1.02
IHex-125×6-1.60-90	819	872	1.06	813	0.99	859	1.05	714	1.05	824	1.01
IHex-125×6-1.60-135	808	860	1.06	812	1.01	859	1.06	714	1.04	824	1.02
IHex-150×6-1.80-90	843	898	1.07	813	0.96	859	1.02	714	1.08	825	0.98
IHex-150×6-1.80-135	840	885	1.05	800	0.95	854	1.02	707	1.08	811	0.97
IHex-160×6-1.90-90	821	868	1.06	804	0.98	856	1.04	709	1.05	815	0.99
IHex-160×6-1.90-135	809	847	1.05	792	0.98	851	1.05	703	1.04	803	0.99
IHex-165×6-1.85-90	805	851	1.06	804	1.00	856	1.06	709	1.03	815	1.01
IHex-165×6-1.85-135	801	845	1.05	801	1.00	855	1.07	708	1.03	813	1.01
IHex-185×6-2.15-90	827	880	1.06	812	0.98	859	1.04	714	1.06	824	1.00
IHex-185×6-2.15-135	818	871	1.06	813	0.99	859	1.05	714	1.05	824	1.01
IHex-185×6-1.90-90	822	885	1.08	826	1.00	864	1.05	721	1.05	838	1.02

IHex-185×6-1.90-135	819	876	1.07	818	1.00	861	1.05	717	1.05	829	1.01
IHex-225×6-2.15-90	818	868	1.06	809	0.99	857	1.05	712	1.05	820	1.00
IHex-225×6-2.15-135	809	849	1.05	795	0.98	852	1.05	704	1.04	806	1.00
IHex-150×10-1.70-90	802	845	1.05	800	1.00	854	1.07	707	1.03	811	1.01
IHex-150×10-1.70-135	810	863	1.07	813	1.00	859	1.06	714	1.04	825	1.02
IHex-160×10-1.50-90	824	879	1.07	815	0.99	860	1.04	715	1.06	826	1.00
IHex-160×10-1.50-135	821	878	1.07	818	1.00	861	1.05	717	1.05	829	1.01
IHex-170×10-2.00-90	825	872	1.06	804	0.97	856	1.04	709	1.06	815	0.99
IHex-170×10-2.00-135	822	871	1.06	807	0.98	857	1.04	711	1.05	818	1.00
CF1-145×6-1.75-C5	827	872	1.05	801	0.97	855	1.03	714	0.86	843	1.06
CF1-145×6-1.75-C7	846	895	1.06	805	0.95	856	1.01	707	0.84	830	1.08
CF2-145×6-1.75-C3	840	885	1.05	800	0.95	854	1.02	710	0.84	816	1.08
CF2-145×6-1.75-C6	843	898	1.07	813	0.96	859	1.02	707	0.85	811	1.08
CF2-220×6-2.00-C4	798	849	1.06	812	1.02	859	1.08	714	0.89	825	1.02
CF2-220×6-2.00-C7	818	868	1.06	809	0.99	857	1.05	713	0.87	823	1.05
CF2-145×10-1.75-C4	802	845	1.05	800	1.00	854	1.07	712	0.88	820	1.03
CF2-145×10-1.75-C7	810	863	1.07	813	1.00	859	1.06	707	0.88	811	1.04
				Mean	0.98	Mean	1.05	Mean	0.87	Mean	1.00
				CoV	0.019	CoV	0.015	CoV	0.016	CoV	0.019

Table 6 Measured initial local geometric imperfection

Section	λ_p	ω_0 (mm)	$\omega_{EN\text{-}s}$ (mm)	$\omega_{EN\text{-}L}$ (mm)	$\omega_{EC3\text{-}5}$ (mm)	$\omega_0/\omega_{EN\text{-}s}$	$\omega_0/\omega_{EN\text{-}l}$	$\omega_0/\omega_{EC3\text{-}5}$
IHex-70×6-1.45	0.26	0.21	0.33	0.38	0.21	0.64	0.55	1.02
IHex-70×6-1.50	0.26	0.22	0.28	0.38	0.18	0.79	0.58	1.24
IHex-70×6-1.50#	0.25	0.18	0.28	0.37	0.18	0.64	0.49	1.02
IHex-70×6-1.55	0.27	0.15	0.21	0.39	0.13	0.71	0.38	1.12
IHex-70×6-1.55#	0.26	0.16	0.21	0.39	0.13	0.76	0.41	1.22
IHex-70×6-1.60	0.26	0.25	0.18	0.38	0.11	1.39	0.66	2.26
IHex-125×6-1.80	0.57	0.26	0.46	0.84	0.29	0.57	0.31	0.90
IHex-125×6-1.80#	0.57	0.25	0.46	0.84	0.29	0.54	0.30	0.87
IHex-125×6-1.60	0.57	0.28	0.75	0.85	0.47	0.37	0.33	0.59
IHex-150×6-1.80	0.70	0.31	0.61	1.03	0.38	0.51	0.30	0.81
IHex-160×6-1.90	0.75	0.42	0.62	1.11	0.39	0.68	0.38	1.08
IHex-160×6-1.90#	0.75	0.44	0.62	1.11	0.39	0.71	0.40	1.13
IHex-165×6-1.85	0.78	0.51	0.69	1.16	0.43	0.74	0.44	1.19
IHex-185×6-2.15	0.89	0.35	0.55	1.31	0.35	0.64	0.27	1.01
IHex-185×6-1.90	0.89	0.55	0.79	1.32	0.50	0.70	0.42	1.11
IHex-225×6-2.15	1.10	0.62	0.72	1.62	0.45	0.86	0.38	1.37
IHex-225×6-2.15#	1.10	0.58	0.72	1.62	0.45	0.81	0.36	1.29
IHex-150×10-1.70	0.38	0.26	0.47	0.94	0.30	0.55	0.28	0.88
IHex-160×10-1.50	0.39	0.25	0.82	0.96	0.52	0.30	0.26	0.49
IHex-170×10-2.00	0.44	0.22	0.33	1.10	0.21	0.67	0.20	1.07

Note: # indicates the repeated test

Table 7 Summary of the HSS cold-formed IHexHS stub column test results.

Specimens	$N_{u,test}$ (kN)	δ_u (mm)	$N_{u,test}$ /Af_y	Failure mode	$N_{u,test}$ / $N_{u,EC3}$	$N_{u,test}$ /$N_{u,AISC}$	$N_{u,test}$ /$N_{u,AS4100}$	$N_{u,test}$ /$N_{u,AISI}$	$N_{u,test}$ / $N_{u,DSM}$	$N_{u,test}$ / $N_{u,CSM}$
IHex-70×6-1.45	1923	5.90	1.05	Yielding	1.07	1.07	1.07	1.07	1.07	1.03
IHex-70×6-1.50	1895	6.03	1.10	Yielding	1.11	1.11	1.11	1.11	1.11	1.07
IHex-70×6-1.50#	1894	6.12	1.10	Yielding	1.12	1.12	1.12	1.12	1.12	1.07
IHex-70×6-1.55	1711	7.78	1.09	Yielding	1.10	1.10	1.10	1.10	1.10	1.05
IHex-70×6-1.55#	1710	7.82	1.09	Yielding	1.11	1.11	1.11	1.11	1.11	1.06
IHex-70×6-1.60	1587	6.39	1.08	Yielding	1.08	1.08	1.08	1.08	1.08	1.03
IHex-125×6-1.80	2643	3.63	0.99	Local bucking	1.01	1.01	1.01	1.01	1.01	1.00
IHex-125×6-1.80#	2642	3.75	0.99	Local bucking	1.01	1.01	1.01	1.01	1.01	1.00
IHex-125×6-1.60	3233	3.40	0.96	Local bucking	0.98	0.98	0.98	0.98	0.98	0.97
IHex-150×6-1.80	3103	3.13	0.95	Local bucking	0.98	0.97	1.01	0.98	0.97	1.00
IHex-160×6-1.90	3102	2.67	0.92	Local bucking	0.96	0.95	1.00	0.96	0.94	1.00
IHex-160×6-1.90#	3108	2.73	0.92	Local bucking	0.96	0.94	1.00	0.96	0.94	1.00
IHex-165×6-1.85	3277	2.80	0.92	Local bucking	0.97	0.95	1.01	0.97	0.94	1.02
IHex-185×6-2.15	2987	2.44	0.87	Local bucking	0.95	0.93	1.01	0.95	0.94	1.02
IHex-185×6-1.90	3671	2.98	0.91	Local bucking	0.99	0.99	1.05	0.99	1.01	1.09
IHex-225×6-2.15	3499	3.61	0.83	Local bucking	0.97	0.94	1.05	0.97	1.01	1.10
IHex-225×6-2.15#	3420	3.55	0.81	Local bucking	0.95	0.92	1.03	0.95	0.99	1.08
IHex-150×10-1.70	5794	8.61	1.07	Yielding	1.09	1.09	1.09	1.09	1.09	1.07
IHex-160×10-1.50	6991	8.23	1.03	Yielding	1.04	1.04	1.04	1.04	1.04	1.03
IHex-170×10-2.00	5404	6.27	1.05	Yielding	1.07	1.07	1.07	1.07	1.07	1.05
				Mean	1.03	1.02	1.05	1.03	1.03	1.04
				CoV	0.059	0.067	0.041	0.059	0.060	0.034
				$Mean^Y$	1.09	1.09	1.09	1.09	1.09	1.05
				CoV^Y	0.022	0.022	0.022	0.022	0.022	0.016
				$Mean^{LB}$	0.98	0.96	1.01	0.98	0.98	1.03
				CoV^{LB}	0.021	0.031	0.020	0.021	0.031	0.041

Note: # indicates the repeated test, ^{Y} indicates the specimen failed by cross-section yielding, ^{LB} indicates the specimen failed by local buckling.

Table 8 Summary of the cross-section yield slenderness limits for internal plate elements under compression

Design standards and methods	Yield slenderness limits	λ_{lim}
EN 1993-1-1 [37]	$b/t \leqslant 42\varepsilon_{EC3}$, $\varepsilon_{EC3}=\sqrt{235/f_y}$, E = 210 GPa	1.405
ANSI/AISC 360-16 [30]	$b/t \leqslant 1.40\varepsilon_{AISC}$, $\varepsilon_{AISC}=\sqrt{E/f_y}$, E = 200 GPa	1.400
EN 1993-1-5 [50]	$\overline{\lambda_p}=\frac{b/t}{28.4\varepsilon\sqrt{k}} \leq 0.5+\sqrt{0.085-0.055\psi}$, $\psi=1$, $\varepsilon_{EC3}=\sqrt{235/f_y}$, $k=4$, E = 210 GPa	1.279
AS 4100 [31]	$b/t \leqslant 35\varepsilon_{AS4100}$, $\varepsilon_{AS4100}=\sqrt{250/f_y}$, E = 200 GPa	1.414
AISI S100-16 [41] AS/NZS 4600 [53]	$\lambda_p=\sqrt{f_y/f_{cr}} \leq 0.673$, $f_{cr}=4\frac{\pi^2 E}{12(1-\nu^2)}(\frac{t}{b})^2$, E = 200 GPa	1.280
DSM [32]	$\lambda_p=\sqrt{f_y/f_{cr}} \leq 0.776$, E = 200 GPa	1.470
CSM [33]	$\lambda_p=\sqrt{f_y/f_{cr}} \leq 0.68$, E = 200 GPa	1.290

Number of Specimen		$N_{u,test}$ /$N_{u,EC3}$	$N_{u,test}$ /$N_{u,AISC}$	$N_{u,test}$ /$N_{u,AS4100}$	$N_{u,test}$ /$N_{u,DSM}$	$N_{u,test}$ /$N_{u,DSM}^{*}$	$N_{u,test}$ /$N_{u,CSM}$	$N_{u,test}$ /$N_{u,CSM}^{*}$	$N_{u,test}$ / $N_{u,ASCE}$	$N_{u,test}$ / $N_{u,Fang}$	$N_{u,test}$ /$N_{u,ASCE}^{*}$	$N_{u,test}$ /$N_{u,ASCE}^{\#}$
Test:13	FE:140											
	Mean	1.03	1.02	1.03	1.03	1.06	1.04	1.04	1.02	1.05	1.05	1.04
	CoV	0.043	0.048	0.042	0.045	0.030	0.025	0.030	0.052	0.031	0.031	0.039
	$k_{d,n}$	3.157	3.157	3.157	3.157	3.157	3.157	3.157	3.157	3.157	3.157	3.157
	b	1.009	1.002	1.011	1.006	1.059	1.036	1.049	0.994	1.043	1.040	1.026
	V_{δ}	0.044	0.048	0.042	0.047	0.030	0.025	0.030	0.053	0.031	0.032	0.039
	V_r	0.094	0.096	0.093	0.095	0.088	0.087	0.088	0.098	0.088	0.088	0.092
	γ_{M0}	1.15	1.15	1.14	1.18	1.11	1.13	1.12	1.18	1.13	1.13	1.14